A facile one-pot synthesis of $Cu_3(PO_4)_2/CuWO_4$ composite for efficient degradation of tetracycline in water: Unraveling the origin of synergistic interactions between the catalyst components

Mateusz Rozmyślak[a], Kamila Sobańska[b], Grzegorz Nowaczyk[c], Adam Kubiak[a], Marcin Frankowski[a], Piotr Pietrzyk[b], Lukasz Wolski[a,*]

[a] *Faculty of Chemistry, Adam Mickiewicz University, ul. Uniwersytetu Poznańskiego 8, 61-614 Poznań, Poland*

[b] *Faculty of Chemistry, Jagiellonian University, ul. Gronostajowa 2, 30-387 Kraków, Poland*

[c] *NanoBioMedical Centre, Adam Mickiewicz University, ul. Wszechnicy Piastowskiej 3, 61-614 Poznań, Poland*

** corresponding author: wolski.lukasz@amu.edu.pl (L. Wolski)*

Abstract:

This study presents a $Cu_3(PO_4)_2/CuWO_4$ composite catalyst (CuPW-1/1), synthesized using a facile co-precipitation method, as a promising catalyst for efficient degradation of tetracycline (TC) in water via H_2O_2-based advanced oxidation processes (AOPs). In a Fenton-like process, CuPW-1/1 was found to be 19 and 66 times more efficient in TC degradation than $CuWO_4$ and $Cu_3(PO_4)_2$, respectively. Moreover, the efficiency of the CuPW-1/1 composite in TC degradation can be further enhanced upon exposure of the reaction medium to ultraviolet (UV) light, achieving more than 90% antibiotic removal in just 30 minutes of the reaction at very low catalyst loading and H_2O_2 dosage. The strongly enhanced activity of the composite catalyst in a Fenton-like process originated from the unique surface properties of this material which enabled a high dispersion of the main active component responsible for the activation of H_2O_2 ($Cu_3(PO_4)_2$) and provided strong interface contact between copper(II) phosphate and copper(II) tungstate, promoting more efficient degradation of TC in a photocatalytic and photo-assisted Fenton-like processes due to the formation of type I heterojunction. The main oxidizing species responsible for the highly efficient degradation and mineralization of TC were hydroxyl radicals. Furthermore, it was established that the CuPW-1/1 composite can efficiently degrade TC in a complex water matrix and can be successfully reused several times without any significant decrease in its efficiency. The results of this study may have a significant impact on the development of new catalysts for H_2O_2-based AOPs addressed to water treatment under environmentally relevant conditions.

Key words:

Copper-based composite catalysts; photo-assisted Fenton-like process; removal of tetracycline; photocatalytic degradation.

1. Introduction

Tetracycline (TC) is one of the most commonly prescribed antibiotics in modern medicine [1]. Nowadays, this chemical compound is frequently detected in both wastewater and surface water, where it occurs at concentrations ranging from trace levels (ng/L) to tens of micrograms per liter, particularly in areas near livestock farms and pharmaceutical facilities [2,3]. Much higher concentrations of this drug have been detected in effluents from pharmaceutical wastewater treatment plants (up to 32.0 mg/L) [4,5]. This situation is alarming, as even trace amounts of antibiotics discharged into the environment can contribute to the development of antibiotic-resistant bacteria, leading to increased mortality and morbidity [6]. Therefore, the development of highly efficient methods that allow for the avoidance of discharging antibiotics into the environment from wastewater treatment plants is one of the most important environmental issues, crucial from the perspective of protecting human health and aquatic life.

Among various methods, advanced oxidation processes (AOPs) have emerged as an auspicious approach to achieve rapid and efficient degradation of organic pollutants in water, due to the formation of highly oxidizing and non-selective reactive oxygen species (ROS), such as hydroxyl radicals ($^{\bullet}OH$) [7]. One of the most widely investigated AOPs are Fenton, and Fenton-like processes in which ROS are formed upon catalytic activation of hydrogen peroxide [8]. To date, the most commonly used heterogeneous catalysts have been based on nanomaterials containing iron or copper oxides [9,10]. In recent years, increasing attention is being directed towards the development of catalysts based on insoluble metal salts such as copper(II) tungstate ($CuWO_4$) or copper(II) phosphate ($Cu_3(PO_4)_2$). $CuWO_4$ is a semiconducting material characterized by a narrow band gap (ca. 2.2-2.4 eV), low toxicity, and high stability against photo-corrosion and chemical corrosion in a neutral and acidic medium [11]. To date, this material has been successfully used as a photocatalyst for the

production of hydrogen [11], and the photocatalytic degradation of various organic pollutants, including methylene blue [12–14] and tetracycline [15]. Although there are no reports on the direct application of $CuWO_4$ in Fenton-like processes, data from the previous literature reveal that the efficiency of pollutant degradation in the presence of $CuWO_4$ as a photocatalyst can be significantly improved by adding H_2O_2 to the reaction medium. For example, previous studies have shown that $CuWO_4$ nanoparticles achieved complete degradation of methylene blue (MB) within 30 minutes and methyl orange (MO) within 75 minutes when the reaction was performed in the presence of H_2O_2 and under exposure to sunlight [16]. Similarly to $CuWO_4$, $Cu_3(PO_4)_2$ has also been recognized as a promising catalyst for the degradation of organic pollutants via photo-assisted Fenton-like processes (e.g., ciprofloxacin [17], and Rhodamine B [18]). For example, recent studies by Rozmyślak et al. [17] revealed that $Cu_3(PO_4)_2$ exhibits ca. 7 times higher activity in the degradation of ciprofloxacin in the presence of H_2O_2 than commercial CuO, and it is several times more active in this process than other metal phosphates. Recently, Chen et al. [18] have observed a significant enhancement of $Cu_3(PO_4)_2$ activity in Fenton-like degradation of Rhodamine B and Rhodamine 6G upon exposure to light.

A notable strategy to improve the catalytic activity of $CuWO_4$ and $Cu_3(PO_4)_2$ involves the formation of composites with other inorganic materials. For example, $CuWO_4$ has been successfully coupled with various semiconductors to improve its activity in photocatalytic processes (e.g., WO_3 [19], $NiFe_2O_4$ [20], MIL-101(Fe) [21], Bi_2WO_6 [22], and ZnO [14]). Recent studies by He et al. [23] revealed that nanocomposites containing TiO_2 and $CuWO_4$ exhibit a much higher efficiency in photocatalytic degradation of atrazine than the individual components due to the enhanced efficiency of charge separation and more efficient formation of ROS upon exposure to light. Regarding the $Cu_3(PO_4)_2$-based composites, Subalakshmi et al. [24] revealed that deposition of $Cu_3(PO_4)_2$ on the surface of MgO enabled much higher activity in photocatalytic degradation of amaranth dye than that observed for pristine MgO and

$Cu_3(PO_4)_2$ materials. However, to our knowledge, there are no reports in the literature related to the development of $CuWO_4/Cu_3(PO_4)_2$ composites and their application in the degradation of antibiotic pollutants via Fenton-like or photo-assisted Fenton-like reactions. Based on the data from the previous literature described above, it was hypothesized that the unique ability of $CuWO_4$ and $Cu_3(PO_4)_2$ catalysts to activate H_2O_2 towards formation of ROS via Fenton-like process and photocatalytic properties of these materials make them interesting candidates for the application in photo-assisted Fenton process, in which the efficiency of radicals formation via Fenton-like mechanism will be significantly improved upon exposure of the reaction medium to ultraviolet (UV) light. Furthermore, it was expected that $Cu_3(PO_4)_2$ and $CuWO_4$ would form a heterojunction that facilitates the separation of photo-excited charge carriers in these semiconductors, leading to improved catalytic activity.

This study aims to synthesize and in-depth characterize new composite catalysts based on $CuWO_4$ and $Cu_3(PO_4)_2$, prepared via a facile one-pot co-precipitation approach, for the degradation of tetracycline in the presence of hydrogen peroxide as an oxidant. To the best of our knowledge, this is the first study to investigate such composite catalysts in H_2O_2-based AOPs. Particular attention was paid to evaluating the catalytic activity of the as-prepared materials in Fenton-like, photocatalytic, and photo-assisted Fenton-like processes, unraveling the nature of synergistic interaction between individual components of the catalysts, and identification of the primary reactive species formed upon catalytic activation of H_2O_2 in the dark and upon exposure to UV light (Fenton-like vs. photo-assisted Fenton-like processes). The studies also included an evaluation of the role of various ROS in the degradation of tetracycline and the evaluation of its degradation pathways based on research using liquid chromatography-mass spectrometry (LC-MS) analytical technique.

2. Experimental

2.1. Chemicals and reagents

Copper(II) nitrate trihydrate ($Cu(NO_3)_2 \cdot 3H_2O$, Sigma-Aldrich, 99-104%), sodium phosphate dibasic (Na_2HPO_4, Sigma-Aldrich, 98-100.5%), sodium tungstate dihydrate ($Na_2WO_4 \cdot 2H_2O$, Sigma-Aldrich, ≥99%), tetracycline hydrochloride ($C_{22}H_{24}N_2O_8 \cdot HCl$, Sigma-Aldrich, ≥95%), hydrogen peroxide (H_2O_2, Sigma-Aldrich, 30%), sodium azide (NaN_3, Sigma-Aldrich, ≥99.5%), chloroform ($CHCl_3$, Honeywell, ≥99.8%), dimethyl sulfoxide (DMSO, $(CH_3)_2SO$, Sigma-Aldrich, ≥99.5%), barium sulfate ($BaSO_4$, Nacalai tesque, ≥98), nitric acid (HNO_3, Sigma-Aldrich, ≥65%), 5,5-dimethyl-1-pyrroline N-oxide (DMPO, Sigma-Aldrich, ≥97%), 2,2,6,6-tetramethylpiperidine (TEMP, Sigma-Aldrich, ≥99%) were used without further purification. Deionized water (DI) was used throughout this study.

2.2. Synthesis of the catalysts

All materials were synthesized by the simple precipitation method. For the preparation of $Cu_3(PO_4)_2$, 5.71 g (23.64 mmol) of $Cu(NO_3)_2 \cdot 3H_2O$ and 4.50 g (31.70 mmol) of Na_2HPO_4 were dissolved in 118 and 158 mL of DI water, respectively. Both solutions were stirred until all salts were fully dissolved. Subsequently, the solution of sodium phosphate dibasic was added to the solution containing copper(II) nitrate trihydrate. The precipitation reaction occurred immediately upon mixing, leading to the obtainment of a light-blue precipitate. The mixture was intensively agitated for 1 hour at room temperature to ensure complete precipitation of metal ions. Afterwards, the precipitate was separated by centrifugation, washed with deionized water, and dried for 24 hours at 80 °C.

To synthesize $CuWO_4$, 2.33 g (9.64 mmol) of $Cu(NO_3)_2 \cdot 3H_2O$ and 3.18 g (9.64 mmol) of $Na_2WO_4 \cdot 2H_2O$ were dissolved in 48 mL of DI water each. The solutions were stirred until transparent and homogeneous solutions were obtained. Then, the solution containing sodium tungstate dihydrate was added to the copper(II) nitrate trihydrate solution under continuous stirring. A light-green precipitate immediately formed after mixing both solutions. Following

1 hour of intensive agitation, the precipitate was separated by centrifugation, washed with deionized water, and dried for 24 hours at 80 °C.

For the synthesis of a composite catalyst containing $Cu_3(PO_4)_2$ and $CuWO_4$ with an assumed mass ratio equal to 1:1 (sample labelled as CuPW-1/1), 2.30 g (9.52 mmol) of $Cu(NO_3)_2 \cdot 3H_2O$ were dissolved in 48 mL of DI water. At the same time, 0.90 g (6.34 mmol) of Na_2HPO_4 and 1.56 g (4.73 mmol) of $Na_2WO_4 \cdot 2H_2O$ were dissolved together in 56 mL of DI water in a separate vessel. Then, the solution containing sodium tungstate dihydrate and sodium phosphate dibasic was stirred into the solution containing copper(II) nitrate trihydrate. The precipitation reaction occurred immediately once these solutions were mixed and led to the obtainment of a light-blue precipitate. After 1 h of intensive agitation, the solid sample was separated by centrifugation, washed with DI water and dried for 24 hours at 80 °C. For comparison purposes, several samples with different $Cu_3(PO_4)_2/CuWO_4$ mass ratio were synthesized using the same experimental procedure. All details related to the synthesis of these samples are provided in Table S1 (see Supplementary Data; SD).

2.3. Characterization of catalysts

All materials prepared in this study were characterized using various experimental techniques, including: X-ray diffraction measurements (XRD; D8 Advance diffractometer, Bruker), low-temperature adsorption-desorption of nitrogen (Autosorb IQ, Quantachrome), inductively coupled plasma optical emission spectrometry (ICP-OES; model 9820, Shimadzu), field-emission scanning electron microscope (FE SEM; Quanta 250 FEG) coupled with energy-dispersive X-ray spectroscopy (SEM-EDS), high-resolution transmission electron microscope (HR TEM; JEOL ARM 200F), attenuated total reflectance – Fourier transform infrared spectroscopy (ATR-FTIR; IRSpirit-X, Shimadzu), diffuse reflectance ultraviolet-visible spectroscopy (DR UV-vis; UV-2600i, Shimadzu), X-ray photoelectron spectroscopy

(XPS; Phoibos150 NAP analyzer, Specs), zeta potential measurements (Zetasizer Nano ZS, Malvern), electron paramagnetic resonance spectroscopy (EPR; MS400 X-band spectrometer, Magnettech). Experimental details related to the characterization of materials using all these techniques are provided in the extended experimental section (see SD).

2.4. Catalytic activity test

Catalytic activity tests were performed in a 250 mL beaker under batch conditions, where 7.5 mg of catalyst was dispersed in 200 mL of TC solution (50 mg/L) at room temperature and stirred in the dark for 30 min to establish the adsorption-desorption equilibrium (stirring rate: 600 rpm). Then, 50 µL of H_2O_2 was added to initiate the catalytic reaction. All catalytic tests related to the degradation of TC in the presence of hydrogen peroxide (Fenton-like processes) were performed under dark conditions to avoid photocatalytic degradation of the antibiotic. In the case of photocatalytic and photo-assisted Fenton-like processes, the reactor was irradiated using a homemade light-emitting diode (LED) reactor presented in Fig. S1. The LED light source was based on single LEDs with a wavelength of 365-370, 380-390 (BRIDGELUX, USA). The diodes were placed on an aluminum heat sink using thermally conductive glue (AG TermoGlue, Poland), and then connected in series. Finally, the LEDs were combined with an LED driver (Topxin Electronics Co., China) to give a power of 25 W, which was confirmed using a GB202 wattmeter (GreenBule, China). The efficiency of tetracycline removal was determined using UV-vis spectroscopy (Shimadzu, UV-1900i, Japan). After a selected reaction time, 4 mL of the reaction mixture was collected from the batch reactor using a syringe, and the catalyst was separated by filtration using a syringe filter (Whatman, hydrophobic, PTFE, 0.2 µm). The filtration process through a syringe filter had no impact on the concentration of TC in the filtrate. The efficiency of the antibiotic removal in the presence of H_2O_2 was determined by measuring the absorbance characteristic of TC at 375 nm where no noticeable disruption originating from the presence of hydrogen peroxide

(H_2O_2 dose ranging from 25 to 500 μL of H_2O_2 per 200 mL of TC solution) was observed (Fig. S2).

All experimental details related to the analysis of pathways of tetracycline degradation using LC-MS studies and the analysis of the efficiency of the antibiotic mineralization based on the measurement of total organic carbon (TOC) concentration in the post-reaction mixtures are provided in the extended experimental section (see SD). The extended experimental section also includes description of experiments with the use of reactive oxygen species scavengers, catalytic tests carried out using environmentally relevant water matrices, and reuse tests (stability studies).

3. Results and discussion

3.1. Physicochemical properties of the catalysts

Fig. 1A presents the XRD patterns of the as-prepared catalysts. $Cu_3(PO_4)_2$ and $CuWO_4$ materials exhibited diffraction peaks consistent with the monoclinic structure of $Cu_3(PO_4)_2 \cdot 3H_2O$ (PDF-00-022-0548) and the triclinic structure of $CuWO_4 \cdot 2H_2O$ (PDF-00-033-0503), respectively. The formation of crystalline $CuWO_4$ and $Cu_3(PO_4)_2$ was additionally confirmed by analysis of Fourier transformation (FFT) diffractograms. As shown in Fig. S3, the lattice spacing determined for copper(II) phosphate and copper(II) tungstate was in good agreement with previous literature data [25,26]. In contrast, CuPW-1/1 sample was amorphous as evidenced by both powder XRD and TEM (not shown), which indicates that the $CuWO_4$ and $Cu_3(PO_4)_2$ phases in the composite sample lost long-range crystallinity. The lack of a well-defined diffraction pattern for CuPW-1/1 made it challenging to determine its chemical composition and structure. Therefore, complementary characterization techniques were required to achieve more comprehensive information on the composition of this material.

ATR-FTIR spectroscopy led us to identify the main functional groups in the catalysts. As shown in Fig. 1B, the IR spectrum recorded for $Cu_3(PO_4)_2$ revealed the presence of absorption bands at 604 cm^{-1} and a broad envelope spanning the range of 950-1050 cm^{-1}. The latter corresponds to the asymmetric stretching vibrations of the PO_4^{3-} tetrahedra [27], while the former band is ascribed to bending modes of the phosphate group [28]. In the case of the IR spectrum of $CuWO_4$, one can observe the absorption bands at ca. 562 and 797 cm^{-1}, attributed to the stretching vibrations [29] and the asymmetric stretching [13] modes of the WO_4^{2-} tetrahedral units in $CuWO_4$, respectively. Notably, the IR spectrum recorded for CuPW-1/1 composite showed a superposition of all vibrational signatures of both individual components (bands at 562, 604, 797, and 950-1050 cm^{-1}), confirming the presence of both types of PO_4^{2-} and WO_4^{2-} structural units in the composite material.

Further indication about the composite catalyst composition was obtained with XPS measurements. As shown in Fig. 2, XPS spectra of all materials in the Cu2p region reveal the presence of peaks at ca. 955.4 and 935.3 eV assigned to $Cu2p_{3/2}$ and $Cu2p_{1/2}$ spectral components characteristic of Cu^{2+} species [30]. For all materials, one can also observe two additional peaks at ca. 962.9 and 942.9 eV, which are typically referred to copper satellites observed for samples containing Cu^{2+} species [30]. This observation further confirms that all materials contained mainly Cu^{2+} species. Regarding the Cu2p region, it is essential to note that for both $CuWO_4$ and CuPW-1/1 catalysts, a minor tail at approximately 933.1 eV can be observed. Since a similar tail in Cu2p region of XPS spectra was previously reported for other materials containing copper(II) tungstate (e.g., [22] and [31]), we claim that this is a unique feature characteristic of $CuWO_4$ structure, rather than direct evidence for the presence of other copper species in these two samples [32,33].

More pronounced differences were observed in the binding energy regions of P2p and W4f. In the case of the P2p spectra, a signal at 133.6 eV was clearly observed for $Cu_3(PO_4)_2$. According to the literature [34], this peak is characteristic of phosphate species and its presence confirms the successful formation of copper(II) phosphate. A similar peak was also noticed for CuPW-1/1 composite (Fig. 2). Analysis of the W4f binding energy region for $CuWO_4$ and CuPW-1/1 materials revealed the presence of peaks that could be deconvoluted into two spectral components at ca. 38.0 and 35.9 eV, and assigned to $W4f_{7/2}$ and $W4f_{5/2}$ orbitals characteristic of tungstate species [33,35]. Therefore, the XPS data revealed that the $CuWO_4$ phase was successfully obtained during the synthesis of $CuWO_4$ and CuPW-1/1. Moreover, these XPS data clearly indicate that the composite catalyst contained both copper(II) tungstate and copper(II) phosphate. More detailed information on the chemical composition of CuPW-1/1 was provided based on ICP-OES measurements. As indicated by the data shown in Table S2, CuPW-1/1 composite contained 52 wt.% of $Cu_3(PO_4)_2$, implying that the actual composition of the catalyst is very similar to the composition arising from the mixture used during synthesis of the composite.

DR UV-vis spectra of $Cu_3(PO_4)_2$ and $CuWO_4$ exhibit two intense absorption bands typical of Cu^{2+} species: one around 250 nm, attributed to ligand-to-metal charge transfer (LMCT) from O^{2-} to Cu^{2+} [36], and another broad band near 800 nm, associated with d-d transitions of Cu^{2+} in a distorted octahedral environment [37] (Fig. 3). The distortion arises from the interactions between Cu^{2+} and neighboring polyhedral units, such as phosphate groups, leading to deviations from ideal octahedral symmetry [36]. The mixed CuPW-1/1 sample exhibits spectral features of both $Cu_3(PO_4)_2$ and $CuWO_4$, with slight shifts in band positions and intensities, suggesting electronic interactions between phosphate and tungstate species. The band gap values estimated for $CuWO_4$ and $Cu_3(PO_4)_2$ based on the Tauc plot

method revealed that the former material has a much lower band gap than the latter (1.79 vs. 2.60 eV, respectively, Fig. 3B and C).

Fig. S4A presents the nitrogen adsorption-desorption isotherms for the investigated catalysts. It was found that all samples exhibited an isotherm of type IVa characteristic of mesoporous materials [38]. More pronounced differences were observed in the shape of the hysteresis loop, which is associated with the presence of capillary condensation within the pores of the investigated materials. This suggested that the investigated samples differed significantly in terms of porosity. Indeed, as indicated by the pore size distribution (Fig. S4B), the $CuWO_4$ material contained relatively small mesopores with an average diameter of ca. 3 nm. In the case of $Cu_3(PO_4)_2$, both small mesopores with an average size of ca. 3-5 nm, and larger mesopores and even macropores are present. In terms of porosity, the CuPW-1/1 catalyst seems to be more similar to $Cu_3(PO_4)_2$ than $CuWO_4$. CuPW-1/1 contains mainly large mesopores with an average diameter of ca. 35 nm. Still, it also contains some larger meso- and macropores (Fig. S4B). The Brunauer-Emmett-Teller (BET) surface area and average pore size estimated for the catalysts are summarized in Table S3. The highest surface area of 82 m^2/g was observed for $CuWO_4$, while the lowest was characteristic of $Cu_3(PO_4)_2$ (8 m^2/g). CuPW-1/1 had a relatively high surface area of 59 m^2/g, which was in between the values observed for the individual components. This observation further confirms that the nanocomposite consists of two distinct phases, which are fused to form a porous structure.

Significant differences in the morphology of catalysts were also confirmed by SEM. As shown in Fig. 4, $CuWO_4$ catalyst consisted of large aggregates with sharp edges. On the contrary, $Cu_3(PO_4)_2$ consisted of much smaller aggregates with blunt corners and edges. In agreement with conclusions drawn based on nitrogen physisorption, the morphology of CuPW-1/1 on a microscale was more similar to $Cu_3(PO_4)_2$ than $CuWO_4$. However, some noticeable differences were clearly observed at higher magnification, which confirms the higher porosity

of CuPW-1/1 catalyst compared to $Cu_3(PO_4)_2$. This further implies that the nanocomposite exhibits a morphology slightly different from that of the individual components. SEM-EDS elemental mapping led us to observe that Cu, P, and W were homogeneously distributed on the surface of the CuPW-1/1 catalyst (Fig. 4). Based on this information, one can conclude that the $Cu_3(PO_4)_2$ and $CuWO_4$ phases in the composite catalyst were fused to form a porous structure in which no clear separation of individual components was observed. This implies the occurrence of a strong interfacial contact between $Cu_3(PO_4)_2$ and $CuWO_4$ in the CuPW-1/1 catalyst, which is crucial for its reactivity during catalytic and photocatalytic processes.

3.2. Catalytic activity

The catalytic activity of the prepared materials was tested in tetracycline degradation via Fenton-like process (reaction with H_2O_2 as the oxidant, no exposure to UV light). Preliminary tests were performed without H_2O_2 addition to determine the ability of the catalysts to adsorb the antibiotic. As shown in Fig. 5A, both $Cu_3(PO_4)_2$ and $CuWO_4$ exhibited relatively low efficiency in antibiotic removal via adsorption. However, it was found that $Cu_3(PO_4)_2$ adsorbed approximately two times more TC than $CuWO_4$ (ca. 6 vs. 3%, respectively) despite its ten times lower surface area (Table S3). This observation led us to conclude that the surface properties of copper(II) phosphate ensure more favorable conditions for the adsorption of TC molecules, but the high efficiency of the adsorptive removal of TC on the surface of this material is limited by its relatively low surface area. Interestingly, a different phenomenon was observed for the CuPW-1/1 composite, which exhibited a remarkably higher adsorption capacity than the pristine components, and adsorbed ca. 25% of the initial TC molecules after 30 min of stirring in the dark (Fig. 5A). This observation further confirmed significant differences in surface properties of the composite material and its components. As shown in Fig. S5, a strong negative charge accumulates on the surface of $CuWO_4$ under the applied reaction conditions (pH ~ 4.5). According to previous studies, at this pH, tetracycline exists in

the form of neutral zwitterion $TC^{0(+/-)}$ [39,40]. Thus, the accumulation of a strong negative charge on the surface of $CuWO_4$ most probably hinders the efficient adsorption of the antibiotic. Furthermore, the surface of $Cu_3(PO_4)_2$ was positively charged at a pH of ~ 4.5. Still, its ability to adsorb TC was found to be relatively low, most likely due to the low surface area of the pristine copper(II) phosphate. Interestingly, the zeta potential measured for CuPW-1/1 was only slightly negative, falling between the values observed for $CuWO_4$ and $Cu_3(PO_4)_2$. Based on this information, one can expect that shielding a strong negative charge, typical of $CuWO_4$, after forming the composite catalyst with $Cu_3(PO_4)_2$ ensured the most favorable conditions for the fast and efficient adsorption of tetracycline. Thus, the strongly enhanced adsorption capacity of the CuPW-1/1 composite originated from its chemical composition and unique surface properties, where $Cu_3(PO_4)_2$ characterized by a low surface area was finely dispersed on $CuWO_4$ with a much higher surface area, ensuring better availability of the adsorption sites on the surface of $Cu_3(PO_4)_2$ in the composite catalyst for the efficient adsorption of TC molecules. Moreover, based on these observations, one can also conclude that the main component of CuPW-1/1 composite responsible for the efficient adsorption of TC is the phosphate phase $Cu_3(PO_4)_2$.

Concerning the efficiency of TC degradation via the Fenton-like process, experiments carried out without the catalyst and in the presence of H_2O_2 revealed that the antibiotic cannot be oxidized directly by hydrogen peroxide (Fig. 5A). The addition of the synthesized catalysts to the reaction medium resulted in a much more efficient degradation of TC. For all materials, degradation of the antibiotic proceeded according to pseudo-first-order kinetics (Fig. 5B). It was found that both $Cu_3(PO_4)_2$ and $CuWO_4$ exhibited relatively low and comparable TC degradation rates (0.00125 and 0.00435 min^{-1}, respectively). Interestingly, the TC degradation rate observed for the CuPW-1/1 composite was 19 times higher than that established for $CuWO_4$ and 66 times higher than that observed for $Cu_3(PO_4)_2$. Moreover, this composite

material removed more than 90% of the initial TC in just 30 min of the reaction using a relatively low catalyst loading of 0.075 g/L. Based on these observations, one can expect that the strongly enhanced activity of CuPW-1/1 originated from a synergistic interaction between $Cu_3(PO_4)_2$ and $CuWO_4$ forming the composite, which can be affected by the ratio of the components. For this reason, additional catalytic tests were performed using materials with different weight ratios of $Cu_3(PO_4)_2/CuWO_4$, and synthesized by the same co-precipitation method. The chemical composition of these samples is presented in Table S2. All these composite materials exhibited comparable surface areas of ca. 54-58 m^2/g, which were much higher than that observed for the pristine $Cu_3(PO_4)_2$ catalyst (Table S3). As shown in Fig. 5C, a composite containing a relatively small amount of $Cu_3(PO_4)_2$ (sample labelled as CuPW-1/4) was found to be significantly more active than the $CuWO_4$ and $Cu_3(PO_4)_2$ materials used individually; however, its activity was still noticeably lower than that observed for CuPW-1/1. This implies that the addition of a small amount of $Cu_3(PO_4)_2$ to $CuWO_4$ leads to a significant increase in the catalytic activity of the composite material during the degradation of TC via a Fenton-like process. Based on this observation, one can expect that $Cu_3(PO_4)_2$ phase may be determinantal active component responsible for the efficient activation of H_2O_2 towards formation of ROS and subsequent degradation of antibiotic molecules via Fenton-like process under dark conditions. At the same time, $CuWO_4$ plays the role of a support on which the $Cu_3(PO_4)_2$ species are highly dispersed, providing better availability of the active sites on the surface of $Cu_3(PO_4)_2$ for the reagents. Indeed, a further increase in the $Cu_3(PO_4)_2/CuWO_4$ weight ratio to 1/2 resulted in a further increase in the TC degradation rate. Nevertheless, the reaction rate constant established for CuPW-1/2 remained lower than that of CuPW-1/1. When the amount of $Cu_3(PO_4)_2$ in the composite was greater than $CuWO_4$ (sample labelled as CuPW-2/1), the activity of the composite was comparable to CuPW-1/2, but did not exceed the activity of CuPW-1/1. Therefore, the optimal composition of the composite catalyst for achieving the

highest efficiency in the removal of TC in the presence of H_2O_2 is a weight ratio of $CuWO_4/Cu_3(PO_4)_2$ = 1/1. Based on these optimization studies, one can expect that noticeable decrease in the activity of CuPW-1/2 composite when comparing to the most active CuPW-1/1 sample results most probably from a lower loading of $Cu_3(PO_4)_2$ phase in this material, which is determinantal for the efficient activation of H_2O_2 through a Fenton-like process under dark conditions (for more details, please see results presented in the section related to EPR studies). This further implies that $CuWO_4$ phase is less efficient in the formation of strongly oxidizing ROS and the degradation of organic pollutants, but it plays a very important role in improving the activity of copper(II) phosphate in these processes. $CuWO_4$ has a much higher surface area than $Cu_3(PO_4)_2$, and this most likely enables a better dispersion of $Cu_3(PO_4)_2$ in the CuPW composite materials, leading to a better availability of the active surface sites of $Cu_3(PO_4)_2$, which are the most active in catalytic activation of hydrogen peroxide and degradation of TC via a Fenton-like process under dark conditions.

Our preliminary studies also assessed the impact of H_2O_2 dose on the efficiency of TC removal in the presence of the most active material. As shown in Fig. 5D, at the lowest H_2O_2 dose of 25 μL, TC degradation rate was 0.05321 min^{-1}. When the H_2O_2 dose was doubled, the reaction rate increased to 0.07069 min^{-1}. However, an additional increase in H_2O_2 concentration resulted in a decrease in TC removal efficiency. At the highest H_2O_2 dose (500 μL), the reaction rate constant decreased to the final value of 0.02992 min^{-1}. This significant decrease in the efficiency of TC degradation at higher doses of H_2O_2 likely resulted from the scavenging effect of H_2O_2. Numerous authors have revealed that excessive H_2O_2 may scavenge ROS produced upon activation of this oxidant, leading to a decrease in the catalytic activity of various nanomaterials [41]. For example, a similar deactivation effect at high H_2O_2 dosages was observed by Pei et al. [42] in catalytic degradation of 2,4-dichlorophenoxyacetic acid. Thus,

the optimal H_2O_2 dose selected in this study to ensure the highest efficiency of TC degradation via the Fenton-like process was 50 μL of hydrogen peroxide per 200 mL of TC solution.

Previous literature data have revealed that $Cu_3(PO_4)_2$ and $CuWO_4$ are promising photocatalysts that may be applied in the efficient degradation of various pollutants in the presence of UV light [24,43]. Indeed, photocatalytic tests revealed that $Cu_3(PO_4)_2$ and $CuWO_4$ can degrade TC after their excitation with UV light. As indicated in Fig. 6A, $Cu_3(PO_4)_2$ was found to be slightly less active in photocatalytic degradation of TC than $CuWO_4$ ($k = 0.00153$ and 0.00224 min^{-1}, respectively). Similarly to the Fenton-like reactions, CuPW-1/1 outperformed pristine $Cu_3(PO_4)_2$ and $CuWO_4$ significantly in terms of their photocatalytic activity. In the case of the composite sample, the TC degradation rate in a photocatalytic process was approximately 3-4 times higher than that observed for the individual components (Fig. 6A). Based on the above observations, we hypothesized that the strongly enhanced photocatalytic activity of CuPW-1/1 composite material makes it an interesting candidate for application in photo-assisted activation of H_2O_2, where the efficiency of TC degradation could be significantly improved by the cumulative effect of ROS generation both via photocatalytic and Fenton-like reactions. To verify this hypothesis, additional studies have been carried out. In all these experiments, the catalyst dose was reduced to 0.0375 g/L due to the relatively high efficiency of TC degradation with H_2O_2, which could hinder expected synergy. Initial experiments using CuPW-1/1 catalyst in the presence of H_2O_2 or UV light only (Fenton-like vs. photocatalytic process) showed that TC can be degraded, but the rate is relatively low due to very low catalyst dosage (Fig. 6B). A very low efficiency of TC degradation was also observed in a photo-assisted Fenton-like reaction without the catalyst ($k = 0.00127$ min^{-1}, Fig. 6B). This means that UV light itself cannot initiate H_2O_2 decomposition to form ROS capable of oxidizing TC. Interestingly, the situation changed after the admission of CuPW-1/1 catalyst, when a remarkable increase in TC degradation rate was observed under simultaneous action of

H_2O_2 and UV light. In this case, the TC degradation rate was found to be ca. 5 times higher than for the photocatalytic reaction (without H_2O_2) and ca. 4 times higher than for the Fenton-like process (reaction in the dark). Furthermore, the TC degradation rate observed for CPW-1/1 composite in a photo-assisted Fenton-like process was approximately 3 times higher than that established for pristine $CuWO_4$ and $Cu_3(PO_4)_2$ samples applied under the same experimental conditions (Fig. 6C). These results imply that the CuPW-1/1 composite is an auspicious material for the efficient degradation of TC in a photo-assisted activation of H_2O_2 that significantly outperforms pristine components acting separately. Furthermore, experiments with a physical mixture of $Cu_3(PO_4)_2$ and $CuWO_4$ materials revealed that the strongly enhanced activity of the composite results from its unique properties that arise during the co-precipitation of the individual components (Fig. 6C).

Our studies also included the identification of TC degradation products using LC-MS analysis. The mass spectra of the pristine TC solution and all post-reaction mixtures are collected in Fig. S8. The proposed structures of the degradation products, identified based on the m/z values and the data from previous literature, are summarized in Table S4. As shown in Fig. S8, the main m/z peaks observed for TC solution are 447, 428, and 410 [44,45]. No significant changes in the mass spectra were observed for the reactions without a catalyst (Fig. S8). This confirms the conclusions of the UV-vis studies. More pronounced changes in the mass spectra were observed after 30 and 60 min of a photo-assisted Fenton-like process in the presence of CuPW-1/1 composite. In this case, the intensity of the peaks typical of tetracycline was significantly decreased. This was associated with the appearance of several new peaks at m/z = 401, 383, 357, 305, 300, 256, 242, 190, 163, 147, and 104. After 30 min of the reaction, the most intense peaks were at m/z = 147 and 104, implying that the complex structure of TC molecule was efficiently degraded in the presence of CuPW-1/1 catalyst. The possible degradation pathways established based on the LC-MS data and previous literature data are

shown in Fig.7. TOC analyses additionally confirmed efficient degradation of the tetracycline. As indicated in Fig. 6D, the concentration of total organic carbon in a post-reaction mixture after 30 min of the photo-assisted Fenton-like reaction in the presence of CuPW-1/1 composite decreased by ca. 60% (from ca. 25 to ca. 15 mg/L). Interestingly, no significant decrease in TOC value was observed in the reaction without CuPW-1/1 catalyst, confirming that this sample is determinant for efficient activation of H_2O_2 and mineralization of this antibiotic pollutant. To identify the main reactive oxygen species responsible for the efficient degradation of TC, additional catalytic tests were performed in the presence of various ROS scavengers. As shown in Fig. 8A, the most pronounced quenching effect was observed in the presence of sodium azide, which is a singlet oxygen ($^1O_2$) scavenger [46]. A similar phenomenon was also observed in the presence of dimethyl sulfoxide as a hydroxyl radical scavenger [46]. In this case, the TC degradation rate decreased from 0.03346 to 0.02568 min^{-1}. Interestingly, no significant deactivation effect was observed for the reactions when using chloroform as a scavenger for superoxide radical anions ($O_2^{\bullet-}$) [46]. Based on the above information, one can expect that the main oxidizing species responsible for TC degradation are singlet oxygen and hydroxyl radicals.

To further confirm the formation of these highly oxidizing species during H_2O_2 activation, EPR studies with TEMP and DMPO were carried out for the detection of $^1O_2$ and $^{\bullet}OH$, respectively. According to the results presented in Fig. 9A, all catalysts used in this study exhibited a comparable ability to form singlet oxygen upon photo-assisted activation of H_2O_2. Noticeable differences in $^1O_2$ formation were observed only for the photocatalytic reactions (without H_2O_2), where CuPW-1/1 composite was found to be significantly more efficient than $Cu_3(PO_4)_2$ and $CuWO_4$ materials. More pronounced differences were observed in ROS formation during a photo-assisted Fenton-like process, particularly in the activation of H_2O_2 towards the formation of hydroxyl radicals. As shown in Fig. 9B, the EPR signal typical of

DMPO-OH spin adduct observed for CuPW-1/1 was ca. 2 times higher than that established for $Cu_3(PO_4)_2$, and remarkably higher than that for $CuWO_4$. Moreover, it was found that hydroxyl radicals could be formed for all catalysts, both in photocatalytic and Fenton-like processes. Based on these observations, we concluded that hydroxyl radicals are the main oxidizing agents during TC degradation in a photo-assisted Fenton-like process with the CuPW-1/1 composite catalyst. However, a contribution of singlet oxygen to the degradation of this antibiotic pollutant cannot be totally excluded, especially during the photocatalytic process.

To fully understand the origin of the enhanced activity of CuPW-1/1 composite both in photocatalytic process and photo-assisted Fenton-like reaction, positions of valence and conduction bands edges in $Cu_3(PO_4)_2$ and $CuWO_4$ materials were predicted theoretically using the following empirical equations (Eq. 1-2) [47]:

$$E_{VB} = \chi - E_e + 0.5*E_g \qquad \text{[Eq. 1]}$$

$$E_{CB} = E_g - E_{VB} \qquad \text{[Eq. 2]}$$

where χ is the absolute electronegativity of the semiconductor, obtained from the geometric mean of the electronegativity of its constituent atoms (χ values for $Cu_3(PO_4)_2$ and $CuWO_4$ are 6.388 eV and 6.319 eV, respectively); E_g is the band gap of the semiconductor (2.60 and 1.79 eV for $Cu_3(PO_4)_2$ and $CuWO_4$, respectively); E_e is the energy of free electrons vs the hydrogen scale (4.5 eV). χ values for individual components were calculated using the formula [Eq. 3], where A, B, C, … N are the constituent atoms of the semiconductor, and a, b, c, … n are the numbers of each atom in the compound. The electronegativity of each atom (X) in $CuWO_4$ or $Cu_3(PO_4)_2$, namely P, W, O, and Cu, was determined based on the arithmetic mean between the electron affinity (EA) and its first ionization energy (IE) [48] (see Table S5 and Eq. 4).

$$\chi = [X(A)^a\, X(B)^b\, X(C)^c]^{\frac{1}{(a+b+c)}} \qquad \text{[Eq. 3]}$$

$$X = (EA + IE)/2 \qquad \text{[Eq. 4]}$$

The results of these calculations are shown in Fig. 10. The calculated conduction band (CB) edge potential of $CuWO_4$ equaled 0.87 eV, which is less negative than that of $Cu_3(PO_4)_2$ (0.62 eV). The corresponding valence band (VB) edge estimated for $Cu_3(PO_4)_2$ was 3.18 eV, which is more positive than that of $CuWO_4$ (2.66 eV). Based on these data and the alignments of band edges, one can conclude that both materials are capable of oxidizing water by photo-generated holes (h^+) towards the formation of hydroxyl radicals. Both materials are also capable of activating H_2O_2 by photo-generated electrons (e^-) because their CB edge is equal to or lies slightly above the potential necessary for activation of H_2O_2 toward formation of hydroxyl radicals ($H_2O_2/^{\bullet}OH$ = 0.87 eV [49,50]). Therefore, the efficiency of these two pristine materials in the degradation of TC via Fenton-like process should be improved upon exposure of the reaction medium to UV light due to more efficient formation of hydroxyl radicals resulting from the activation of H_2O_2 by photo-excited electrons localized in the conduction band of these semiconductors. Indeed, the experimental data shown in Fig. S10, revealed that the TC degradation rate in a photo-assisted Fenton-like process increased by a factor of ca. 6.5 and 7.5 in the presence of $Cu_3(PO_4)_2$ and $CuWO_4$, respectively, when compared to the activity of these materials in a Fenton-like process carried out in the dark. The more efficient formation of hydroxyl radicals in a photo-assisted Fenton-like process on the surface of these two materials was further confirmed by EPR data presented in Fig. 9B. A noticeable improvement in the efficiency of TC degradation via Fenton-like process upon exposure to UV light was also observed for CuPW-1/1 composite, reaching ca. 3.0 and 2.5 times higher reaction rate constants than those established for the individual components of the composite, namely $Cu_3(PO_4)_2$ and $CuWO_4$, respectively (Fig. S10). Given the band edges alignment between these two semiconductors, one can expect that the most plausible mechanism of the photo-excited charge carriers transfer between $Cu_3(PO_4)_2$ and $CuWO_4$ in the CuPW-1/1 composite under irradiation

with UV light results from the formation of a heterojunction of type I. According to the literature [51,52], this mechanism leads to the accumulation of both photo-excited electrons and holes in $CuWO_4$, and implies that the electron and hole transfer from $Cu_3(PO_4)_2$ to $CuWO_4$ is accelerated under the light excitation conditions. However, since both electron and hole pairs are transferred to $CuWO_4$, they cannot be separated very efficiently. For this reason, the enhancement of TC degradation rate in the presence of CuPW-1/1 composite in a Fenton-like process upon exposure to UV light was slightly lower than that observed for the reactions carried out in the presence of individual components (increase by a factor of approximately 3.5, 6.5 and 7.5 for CuPW-1/1, $Cu_3(PO_4)_2$, and $CuWO_4$, respectively; Fig. S10). Nevertheless, it is important to underline that the TC degradation rate observed for the composite catalyst in the photo-assisted Fenton-like process was still significantly higher than those established for $Cu_3(PO_4)_2$, and $CuWO_4$ used separately. The most plausible mechanism of charge separation contributing to the enhanced activity of CuPW-1/1 composite in a photo-assisted Fenton-like process is presented in Fig 10.

One of the most critical factors affecting the catalytic activity of materials in reactions involving H_2O_2 is the pH of the reaction mixture. Typically, the highest activity in degradation processes occurs under acidic conditions, where many materials exhibit higher efficiency in activating H_2O_2 to form hydroxyl radicals. The experimental data obtained in this study are consistent with previous reports in this field and show that the reaction rate constant observed under native pH (pH ~ 4.5) is approximately twice as much as at pH close to neutral (pH ~ 7) (Fig. 8B). Nevertheless, even under neutral conditions, the catalyst activity remains relatively high when considering such a low catalyst loading (0.0375 g/L).

To evaluate the potential practical application of CuPW-1/1 composite in the degradation of TC in environmentally relevant water matrices, additional experiments were conducted using tap water and river water. The chemical composition of these water samples

is shown in Table S6. Both samples have similar pH values (~ 7.5). However, tap water contains noticeably higher concentrations of inorganic carbon than river water (53 vs. 47 mg/L, respectively). In contrast, river water exhibits a higher concentration of total organic carbon (0.6 mg/L while traces were measured for tap water), and a higher concentration of total nitrogen (3.5 vs. 0.7 mg/L, respectively). As shown in Fig. 8C, the TC degradation rate in tap water and river water was ca. 0.5 times lower than in the case of deionized water at a pH of ~ 7. Interestingly, the TC degradation rate in tap water was even lower than that observed for river water, which contains a higher concentration of total organic carbon and total nitrogen. This shows that these two components are not the most critical factors diminishing the catalytic activity of CuPW-1/1 composite under environmentally relevant conditions. As mentioned above, tap water contained a noticeably higher concentration of inorganic carbon, which is widely reported in the literature as a factor decreasing the activity of various catalysts in the degradation of pollutants using H_2O_2 as the oxidant [53]. It was reported that carbonate species in water may act as scavengers for hydroxyl radicals, leading to a decrease in the efficiency of organics degradation [54]. Based on this information, one can conclude that the CuPW-1/1 composite can degrade TC even in complex water matrices, and the main factor diminishing its catalytic activity is inorganic carbon dissolved in environmentally relevant water samples.

Another factor that significantly impacts the potential application of catalysts for water treatment is their stability. In this study, this feature of CuPW-1/1 composite was investigated by testing the catalyst in several subsequent degradation cycles. As shown in Fig. 8D, the TC degradation rate decreased slightly after each reaction cycle. Nevertheless, after the fifth reaction cycle, it only reduced by ca. 20% as compared to the first cycle, and still enabled a relatively high efficiency of the TC removal after 30 min of the reaction. This slight deactivation effect likely resulted from the partial loss of the catalyst during the reuse procedure and/or leaching of copper species during the reaction, which is commonly observed in

oxidation processes using copper-based catalysts (see e.g., [55]). To evaluate the concentration of leached copper, the post-reaction mixtures after each reuse test were analyzed using ICP-OES. Data obtained from these measurements are summarized in Table S7. As it was expected, the ICP-OES studies confirmed the leaching of copper species from the CuPW-1/1 composite. After the first reaction cycle, the concentration of copper species in treated water was approximately 13 mg/L, while the concentrations of P and W were equal to 4.5 and 13.5 mg/L, respectively. These values are relatively high, but it is important to underline that the reuse tests were carried out using a higher catalyst loading than in all previous experiments to facilitate separation of the catalyst after its reuse and minimize the impact of catalyst loss on the efficiency of TC degradation in further reaction cycles. For the experiments carried out using a low catalyst dosage and environmentally relevant water samples (e.g. river water), the concentration of leached copper species was much lower (ca. 1.59 mg/L; Table S7). In this case, the concentration of leached copper species was lower than the upper limit for copper in drinking water in the European Union (2 mg/L) [56], and only slightly higher than the upper limit established by the U.S. Environmental Protection Agency (EPA) (1.3 mg/L) [56]. Therefore, ICP-OES studies led us to establish that the application of CuPW-1/1 composite leads to generation of secondary pollutants in the form of leached copper species. Still, these metal cations could be potentially eliminated from treated water by an additional water treatment step using various adsorbents like zeolites, metal oxides or polymers, as reported in the previous literature data [56]. As far as the stability of the CuPW-1/1 composite is concerned, it is worth noting that the analysis of a spent catalyst by XRD, ATR-FTIR, and XPS techniques did not reveal any significant changes in its structure. As shown in Fig. S11, the spent catalyst remained amorphous and all IR bands characteristic of its individual components were preserved. Some additional IR bands were noticed and resulted from the presence of adsorbed TC molecules and/or their degradation products on the surface of CuPW-1/1

composite (Fig. S11B). Furthermore, XPS studies did not reveal any noticeable changes in the oxidation state and electronic properties of copper, phosphorus, and tungsten in the spent catalyst (Fig. S11C). These results led us to establish that some Cu, W, and P species are leached from the CuPW-1/1 composite under working conditions, but this leaching process does not cause significant changes in the structure or oxidation state of the components of this catalyst. For this reason, the spent solid material could be easily separated from the post-reaction mixture by centrifugation and successfully applied in the next few reaction cycles. The last factor necessary to be considered is the contribution of the leached copper species to the degradation of TC via photo-assisted Fenton-like process. In this study, the contribution of leached copper ions to the degradation of TC was analyzed based on the experiment in which the solid catalyst was separated from the reaction mixture after 30 min of the adsorption step in the dark and 5 min of the reaction in the presence of H_2O_2 and UV light, and then the process was continued without the solid catalyst. According to the results presented in Fig. S12B, the rate of TC degradation in a reaction mixture after separation of the catalyst was ca. 2 times lower than that established for the reaction carried out in the presence of the catalyst. These experimental data show that the leached copper species act as a homogeneous catalyst and contribute to the degradation of TC, but the presence of a solid material in the reaction mixture is important for ensuring a very high efficiency of the antibiotic degradation via photo-assisted Fenton-like process.

4. Conclusions

The results of this study demonstrate that the $Cu_3(PO_4)_2/CuWO_4$ composite is a promising catalyst for the rapid and efficient degradation of tetracycline in water, even when a small amount of the catalyst was applied under a low concentration of H_2O_2. It was also observed that the efficiency of TC degradation in the presence of the CuPW-1/1 composite via Fenton-like process may be significantly enhanced upon exposure of the reaction medium to

UV light, significantly outperforming the catalytic activity of the individual structural components $CuWO_4$ and $Cu_3(PO_4)_2$. The strongly enhanced activity of the composite catalyst originated from the unique surface properties of this material, which enabled a high dispersion of the main active component responsible for the activation of H_2O_2 in the dark conditions via Fenton-like process (identified as $Cu_3(PO_4)_2$) and provided tight interface contact between copper(II) phosphate and copper(II) tungstate, thus, promoting more efficient degradation of TC in a photocatalytic and photo-assisted Fenton-like processes due to formation of heterojunction of type I. Catalytic tests performed in the presence of ROS scavengers combined with EPR studies indicated hydroxyl radicals as the main oxidizing species responsible for the observed degradation and mineralization of TC. Furthermore, it was established that the CuPW-1/1 composite could efficiently degrade TC in a complex water matrix and could be reused several times without any significant decrease in its efficiency.

The results obtained in this study demonstrate that the synthesis of new copper-based composite catalysts via the facile co-precipitation method is a promising strategy for obtaining highly efficient catalysts for the degradation of antibiotic pollutants through photo-assisted Fenton-like processes. The findings of this study may have a significant impact on the development of new copper-based catalysts for AOPs addressed to water treatment under environmentally benign and environmentally relevant conditions.

Acknowledgments

This work was financially supported by National Science Centre, Poland (grant Sonata no. 2023/51/D/ST5/00216). M. Rozmyślak acknowledges the ID-UB program for financial support of this work (project no. 136/13/SNŚ/0005). The authors thank Dr. Joanna Wolska for conducting the zeta potential measurements.

References

[1] Q. Liao, H. Rong, M. Zhao, H. Luo, Z. Chu, R. Wang, Interaction between tetracycline and microorganisms during wastewater treatment: A review, Sci. Total Environ. 757 (2021) 143981, https://doi.org/10.1016/j.scitotenv.2020.143981.

[2] G. Gopal, S.A. Alex, N. Chandrasekaran, A. Mukherjee, A review on tetracycline removal from aqueous systems by advanced treatment techniques, RSC Adv. 10 (2020) 27081–27095, https://doi.org/10.1039/D0RA04264A.

[3] A. Pena, M. Paulo, L.J.G. Silva, M. Seifrtová, C.M. Lino, P. Solich, Tetracycline antibiotics in hospital and municipal wastewaters: a pilot study in Portugal, Anal. Bioanal. Chem. 396 (2010) 2929–2936, https://doi.org/10.1007/s00216-010-3581-3.

[4] J. Scaria, K.V. Anupama, P.V. Nidheesh, Tetracyclines in the environment: An overview on the occurrence, fate, toxicity, detection, removal methods, and sludge management, Sci. Total Environ. 771 (2021) 145291, https://doi.org/10.1016/j.scitotenv.2021.145291.

[5] J. Hou, C. Wang, D. Mao, Y. Luo, The occurrence and fate of tetracyclines in two pharmaceutical wastewater treatment plants of Northern China, Environ. Sci. Pollut. Res. 23 (2016) 1722–1731, https://doi.org/10.1007/s11356-015-5431-5.

[6] M. Naghavi, S.E. Vollset, K.S. Ikuta, L.R. Swetschinski, A.P. Gray, E.E. Wool, G. Robles Aguilar, et al., Global burden of bacterial antimicrobial resistance 1990–2021: a systematic analysis with forecasts to 2050, Lancet 404 (2024) 1199–1226, https://doi.org/10.1016/S0140-6736(24)01867-1.

[7] S. Li, Y. Wu, H. Zheng, H. Li, Y. Zheng, J. Nan, J. Ma, D. Nagarajan, J.-S. Chang, Antibiotics degradation by advanced oxidation process (AOPs): Recent advances in ecotoxicity and antibiotic-resistance genes induction of degradation products,

Chemosphere 311 (2023) 136977, https://doi.org/10.1016/j.chemosphere.2022.136977.

[8] X. Wang, J. Jing, M. Zhou, R. Dewil, Recent advances in H_2O_2-based advanced oxidation processes for removal of antibiotics from wastewater, Chinese Chem. Lett. 34 (2023) 107621, https://doi.org/10.1016/j.cclet.2022.06.044.

[9] E.C. Okpara, O.B. Wojuola, T.W. Quadri, C.E. Banks, An overview of advanced oxidation processes using copper-based catalytic degradation of organic pollutants in water, Appl. Mater. Today 36 (2024) 102053, https://doi.org/10.1016/j.apmt.2023.102053.

[10] H. Luo, Y. Zeng, D. He, X. Pan, Application of iron-based materials in heterogeneous advanced oxidation processes for wastewater treatment: A review, Chem. Eng. J. 407 (2021) 127191, https://doi.org/10.1016/j.cej.2020.127191.

[11] P. Raizada, S. Sharma, A. Kumar, P. Singh, A.A. Parwaz Khan, A.M. Asiri, Performance improvement strategies of $CuWO_4$ photocatalyst for hydrogen generation and pollutant degradation, J. Environ. Chem. Eng. 8 (2020) 104230, https://doi.org/10.1016/j.jece.2020.104230.

[12] D. Xiang, X. Jin, G. Sun, C. Zhong, S. Gao, Oxygen vacancy engineering of ultra-small $CuWO_4$ nanoparticles for boosting photocatalytic organic pollutant degradation, Dalt. Trans. 53 (2024) 7839–7847, https://doi.org/10.1039/D4DT00628C.

[13] X. Hu, D. Gao, Y. Li, H. Dong, W. Zhou, L. Yang, Y. Zhang, Fabrication of novel $CuWO_4$ nanoparticles (NPs) for photocatalytic degradation of methylene blue in aqueous solution, SN Appl. Sci. 1 (2019) 119, https://doi.org/10.1007/s42452-018-0113-9.

[14] C. Chen, W. Bi, Z. Xia, W. Yuan, L. Li, Hydrothermal Synthesis of the $CuWO_4$/ZnO

Composites with Enhanced Photocatalytic Performance, ACS Omega 5 (2020) 13185–13195, https://doi.org/10.1021/acsomega.0c01220.

[15] T.T. My Hang, N.H. Thao Vy, N.T. Hanh, T.-D. Pham, L.T. Hoang Yen, Facile synthesis of copper tungstate ($CuWO_4$) for novel photocatalytic degradation of tetracycline under visible light, Sustain. Chem. Pharm. 21 (2021) 100407, https://doi.org/10.1016/j.scp.2021.100407.

[16] M. Waimbo, G. Anduwan, O. Renagi, S. Badhula, K. Michael, J. Park, S. Velusamy, Y.S. Kim, Improved charge separation through H_2O_2 assisted copper tungstate for enhanced photocatalytic efficiency for the degradation of organic dyes under simulated sun light, J. Photochem. Photobiol. B Biol. 204 (2020) 111781, https://doi.org/10.1016/j.jphotobiol.2020.111781.

[17] M. Rozmyślak, A. Walkowiak, M. Frankowski, L. Wolski, Copper(II) phosphate as a promising catalyst for the degradation of ciprofloxacin via photo-assisted Fenton-like process, Sci. Rep. 14 (2024) 7007, https://doi.org/10.1038/s41598-024-57542-9.

[18] M. Chen, G. Zhang, Y. Jiang, K. Yin, L. Zhang, H. Li, J. Hao, Fullerene-Directed Synthesis of Flowerlike $Cu_3(PO_4)_2$ Crystals for Efficient Photocatalytic Degradation of Dyes, Langmuir 35 (2019) 8806–8815, https://doi.org/10.1021/acs.langmuir.9b00193.

[19] R. Sharma, N. Islam, A. Priye, D. Kumar, J. Singh, M. Kumar, P.P. Sharma, V. Chauhan, P. Shandilya, Fabrication of dual S-scheme based $CuWO_4$/NiFe/WO_3 heterojunction for visible-light-induced degradation and reduction applications, J. Environ. Chem. Eng. 12 (2024) 112126, https://doi.org/10.1016/j.jece.2024.112126.

[20] U. Kumar, A. Shrivastava, A.K. De, M.R. Pai, I. Sinha, Fenton reaction by H_2O_2 produced on a magnetically recyclable Ag/$CuWO_4$/$NiFe_2O_4$ photocatalyst, Catal. Sci.

Technol. 13 (2023) 2432–2446, https://doi.org/10.1039/D3CY00102D.

[21] M. Khan, M.M. Ahmed, M.N. Akhtar, M. Sajid, N.N. Riaz, M. Asif, M. Kashif, B. Shabbir, K. Ahmad, M. Saeed, M. Shafiq, T. Shabir, Fabrication of $CuWO_4$@MIL-101 (Fe) nanocomposite for efficient OER and photodegradation of methylene blue, Heliyon 10 (2024) e40546, https://doi.org/10.1016/j.heliyon.2024.e40546.

[22] Y. Han, X.-X. Qi, Y.-C. Liu, Y. Wang, Z. Xiang, X. Wang, Preparation of $CuWO_4/Bi_2WO_6$ composite and its sonocatalytic removal of tetracycline by combined persulfate, J. Alloys Compd. 1010 (2025) 177505, https://doi.org/10.1016/j.jallcom.2024.177505.

[23] D. He, Y. Yang, J. Tang, K. Zhou, W. Chen, Y. Chen, Z. Dong, Synergistic effect of TiO_2-$CuWO_4$ on the photocatalytic degradation of atrazine, Environ. Sci. Pollut. Res. 26 (2019) 12359–12367, https://doi.org/10.1007/s11356-019-04686-1.

[24] A. Subalakshmi, B. Kavitha, N. Srinivasan, M. Rajarajan, A. Suganthi, Evaluation of photocatalytic activity of $Cu_3(PO_4)_2$/MgO nanocomposite for the efficient removal of amaranth dye under solar light irradiation, Inorg. Chem. Commun. 161 (2024) 112033, https://doi.org/10.1016/j.inoche.2024.112033.

[25] O.C. Güven, M. Kar, F.D. Koca, Synthesis of Cherry Stalk Extract Based Organic@Inorganic Hybrid Nanoflowers as a Novel Fenton Reagent: Evaluation of Their Antioxidant, Catalytic, and Antimicrobial Activities, J. Inorg. Organomet. Polym. Mater. 32 (2022) 1026–1032, https://doi.org/10.1007/s10904-021-02160-5.

[26] R. Roshani, A. Tadjarodi, A. Ghaffarinejad, The effect of annealing temperature on the structure and supercapacitive properties of copper tungstate, Mater. Lett. 293 (2021) 129644, https://doi.org/10.1016/j.matlet.2021.129644.

[27] H. Wu, J. Song, C. Xie, Y. Hu, S. Liu, B. Han, Preparation of Copper Phosphate from Naturally Occurring Phytic Acid as an Advanced Catalyst for Oxidation of Aromatic Benzyl Compounds, ACS Sustain. Chem. Eng. 6 (2018) 13670–13675, https://doi.org/10.1021/acssuschemeng.8b04193.

[28] J. Jiao, X. Xin, X. Wang, Z. Xie, C. Xia, W. Pan, Self-assembly of biosurfactant–inorganic hybrid nanoflowers as efficient catalysts for degradation of cationic dyes, RSC Adv. 7 (2017) 43474–43482, https://doi.org/10.1039/C7RA06592B.

[29] R. Chen, X. Dou, J. Xia, Y. Chen, H. Shi, Boosting peroxymonosulfate activation over $Bi_2MoO_6/CuWO_4$ to rapidly degrade tetracycline: Intermediates and mechanism, Sep. Purif. Technol. 296 (2022) 121345, https://doi.org/10.1016/j.seppur.2022.121345.

[30] A. Samal, D.P. Das, G. Madras, Repercussion of Solid state vs. Liquid state synthesized p-n heterojunction RGO-copper phosphate on proton reduction potential in water, Sci. Rep. 8 (2018) 2881, https://doi.org/10.1038/s41598-018-21239-7.

[31] O.Y. Khyzhun, T. Strunskus, S. Cramm, Y.M. Solonin, Electronic structure of $CuWO_4$: XPS, XES and NEXAFS studies, J. Alloys Compd. 389 (2005) 14–20, https://doi.org/10.1016/j.jallcom.2004.08.013.

[32] A. K., C.S.R. Vusa, S. Berchmans, Enhanced peroxidase-like activity of $CuWO_4$ nanoparticles for the detection of NADH and hydrogen peroxide, Sensors Actuators B Chem. 253 (2017) 723–730, https://doi.org/10.1016/j.snb.2017.06.175.

[33] Y. Cui, C. Lin, M. Li, N. Zhu, J. Meng, J. Zhao, $CuWO_4$/CuS heterojunction photocatalyst for the application of visible-light-driven photodegradation of dye pollutions, J. Alloys Compd. 893 (2022) 162181,

https://doi.org/10.1016/j.jallcom.2021.162181.

[34] C. Ma, Y. Zhang, C. Yang, Y. Zhang, M. Zhang, J. Tang, Cetyl trimethyl ammonium bromide-activated lipase from Aspergillus oryzae immobilized with $Cu_3(PO_4)_2 \cdot 3H_2O$ via biomineralization for hydrolysis of olive oil, LWT 159 (2022) 113204, https://doi.org/10.1016/j.lwt.2022.113204.

[35] S. Somacescu, A. Stanoiu, I.V. Dinu, J.M. Calderon-Moreno, O.G. Florea, M. Florea, P. Osiceanu, C.E. Simion, $CuWO_4$ with CuO and $Cu(OH)_2$ Native Surface Layers for H_2S Detection under in-Field Conditions, Materials. 14 (2021) 465, https://doi.org/10.3390/ma14020465.

[36] Z. Hua, B. Li, L. Li, X. Yin, K. Chen, W. Wang, Designing a Novel Photothermal Material of Hierarchical Microstructured Copper Phosphate for Solar Evaporation Enhancement, J. Phys. Chem. C 121 (2017) 60–69, https://doi.org/10.1021/acs.jpcc.6b08975.

[37] A. Le Nestour, M. Gaudon, G. Villeneuve, R. Andriessen, A. Demourgues, Steric and Electronic Effects Relating to the Cu^{2+} Jahn−Teller Distortion in $Zn_{1-x}Cu_xAl_2O_4$ Spinels, Inorg. Chem. 46 (2007) 2645–2658, https://doi.org/10.1021/ic062329c.

[38] M. Thommes, K. Kaneko, A. V. Neimark, J.P. Olivier, F. Rodriguez-Reinoso, J. Rouquerol, K.S.W. Sing, Physisorption of gases, with special reference to the evaluation of surface area and pore size distribution (IUPAC Technical Report), Pure Appl. Chem. 87 (2015) 1051–1069, https://doi.org/10.1515/pac-2014-1117.

[39] J. Jin, Z. Yang, W. Xiong, Y. Zhou, R. Xu, Y. Zhang, J. Cao, X. Li, C. Zhou, Cu and Co nanoparticles co-doped MIL-101 as a novel adsorbent for efficient removal of tetracycline from aqueous solutions, Sci. Total Environ. 650 (2019) 408–418,

https://doi.org/10.1016/j.scitotenv.2018.08.434.

[40] J. Wolska, A. Zioła-Frankowska, J. Jenczyk, A. Zaleta, K. Sobańska, P. Pietrzyk, L. Wolski, Development of adsorbents based on phosphate-containing hyper-cross-linked polymers for selective removal of tetracycline from water: Unveiling the role of phosphate groups in adsorption, Sep. Purif. Technol. 367 (2025) 132846, https://doi.org/10.1016/j.seppur.2025.132846.

[41] D.D. Dionysiou, M.T. Suidan, I. Baudin, J.-M. Laîné, Effect of hydrogen peroxide on the destruction of organic contaminants-synergism and inhibition in a continuous-mode photocatalytic reactor, Appl. Catal. B Environ. 50 (2004) 259–269, https://doi.org/10.1016/j.apcatb.2004.01.022.

[42] C.C. Pei, W. Chu, The photocatalyic degradation and modeling of 2,4-Dichlorophenoxyacetic acid by bismuth tungstate/peroxide, Chem. Eng. J. 223 (2013) 665–669, https://doi.org/10.1016/j.cej.2013.02.125.

[43] S.M. Hosseinpour-mashkani, A. Sobhani-Nasab, Simple synthesis and characterization of copper tungstate nanoparticles: investigation of surfactant effect and its photocatalyst application, J. Mater. Sci. Mater. Electron. 27 (2016) 7548–7553, https://doi.org/10.1007/s10854-016-4735-7.

[44] I. Dalmázio, M.O. Almeida, R. Augusti, T.M.A. Alves, Monitoring the degradation of tetracycline by ozone in aqueous medium via atmospheric pressure ionization mass spectrometry, J. Am. Soc. Mass Spectrom. 18 (2007) 679–687, https://doi.org/10.1016/j.jasms.2006.12.001.

[45] W.R. Chen, C.H. Huang, Transformation kinetics and pathways of tetracycline antibiotics with manganese oxide, Environ. Pollut. 159 (2011) 1092–1100,

https://doi.org/10.1016/j.envpol.2011.02.027.

[46] C. Zhang, L. Liu, Y. Pan, R. Qin, W. Wang, M. Zhou, Y. Zhang, Detection methodologies and mechanisms of reactive oxygen species generated in Fenton/Fenton-like processes, Sep. Purif. Technol. 355 (2025) 129578, https://doi.org/10.1016/j.seppur.2024.129578.

[47] S. Zhou, Y. Wang, G. Zhao, C. Li, L. Liu, F. Jiao, Enhanced visible light photocatalytic degradation of rhodamine B by Z-scheme $CuWO_4$/g-C_3N_4 heterojunction, J. Mater. Sci. Mater. Electron. 32 (2021) 2731–2743, https://doi.org/10.1007/s10854-020-05003-0.

[48] J.P. Fuentes, S. Jadoun, O. Yepsen, H.D. Mansilla, J. Yáñez, Prediction of band edge potentials and reaction products in photocatalytic copper and iron sulfides, Photochem. Photobiol. Sci. 22 (2023) 1855–1864, https://doi.org/10.1007/s43630-023-00415-3.

[49] F. Deng, X. Lu, X. Pei, X. Luo, S. Luo, D.D. Dionysiou, Fabrication of ternary reduced graphene oxide/SnS_2/$ZnFe_2O_4$ composite for high visible-light photocatalytic activity and stability, J. Hazard. Mater. 332 (2017) 149–161, https://doi.org/10.1016/j.jhazmat.2017.01.058.

[50] Y. Cao, Y. Ren, J. Zhang, T. Xie, Y. Lin, Activation of H_2O_2 by photo-generated electrons for enhanced visible light driven methylene blue degradation with $ZnFe_2O_4$/$BiVO_4$ heterojunction, Opt. Mater. 121 (2021) 111637, https://doi.org/10.1016/j.optmat.2021.111637.

[51] J. Low, J. Yu, M. Jaroniec, S. Wageh, A.A. Al-Ghamdi, Heterojunction Photocatalysts, Adv. Mater. 29 (2017) 1–20, https://doi.org/10.1002/adma.201601694.

[52] M. Lin, H. Chen, Z. Zhang, X. Wang, Engineering interface structures for heterojunction photocatalysts, Phys. Chem. Chem. Phys. 25 (2023) 4388–4407,

https://doi.org/10.1039/d2cp05281d.

[53] S. Ziembowicz, M. Kida, Limitations and future directions of application of the Fenton-like process in micropollutants degradation in water and wastewater treatment: A critical review, Chemosphere 296 (2022) 134041, https://doi.org/10.1016/j.chemosphere.2022.134041.

[54] S. Giannakis, M.I.P. López, D. Spuhler, J.A.S. Pérez, P.F. Ibáñez, C. Pulgarin, Solar disinfection is an augmentable, in situ-generated photo-Fenton reaction-Part 2: A review of the applications for drinking water and wastewater disinfection, Appl. Catal. B Environ. 198 (2016) 431–446, https://doi.org/10.1016/j.apcatb.2016.06.007.

[55] L. Lyu, L. Zhang, C. Hu, Enhanced Fenton-like degradation of pharmaceuticals over framework copper species in copper-doped mesoporous silica microspheres, Chem. Eng. J. 274 (2015) 298–306, https://doi.org/10.1016/j.cej.2015.03.137.

[56] E.C. Emenike, A.G. Adeniyi, P.E. Omuku, K.C. Okwu, K.O. Iwuozor, Recent advances in nano-adsorbents for the sequestration of copper from water, J. Water Process Eng. 47 (2022) 102715, https://doi.org/10.1016/j.jwpe.2022.102715.

Caption to Figures

Fig. 1. (A) Powder XRD diffractograms and **(B)** ATR-FTIR spectra of the catalysts.

Fig. 2. XPS spectra of $CuWO_4$, $Cu_3(PO_4)_2$ and CuPW-1/1catalysts in different binding energy regions: **(A)** Cu2p, **(B)** P 2p + Cu 3s, and **(C)** W 4f.

Fig. 3. (A) DR UV-vis spectra of the catalysts. Tauc's plot used for the estimation of band gap energy for **(B)** $CuWO_4$ and **(C)** $Cu_3(PO_4)_2$.

Fig. 4. Scanning Electron Microscopy analysis of synthesized catalysts combined with EDX elemental mapping of CuPW-1/1.

Fig. 5. (A) Efficiency of TC removal over time for $Cu_3(PO_4)_2$, $CuWO_4$ and CuPW-1/1 samples in a Fenton-like process (no exposure to UV light), including a control experiment without a catalyst. For all experiments, pre-adsorption of the pollutant was performed for 30 min before addition of H_2O_2 to assess the ability of a given catalyst to adsorb TC. Time when H_2O_2 was added to the reaction medium is marked as dashed line. **(B)** Pseudo-first order kinetics plot used to estimate TC degradation rate in the presence of investigated copper-based catalysts in a Fenton-like process. **(C)** Influence of chemical composition of CuPW composites on the TC degradation rate in the presence of H_2O_2. Pseudo-first-order kinetic plots are shown in Fig. S6A. **(D)** TC degradation rate in the presence of various concentrations of H_2O_2 for the CuPW-1/1 catalyst in a Fenton-like process. Changes in TC concentration during the reaction and the pseudo-first-order kinetic plots are shown in Fig. S6B and C, respectively. *Reaction conditions*: catalyst (15 mg), TC solution in DI water (200 mL, 50 mg/L), H_2O_2 (50 µL, or other if indicated), room temperature (r.t.), 600 rpm, without pH control (native pH ~ 4.5), all reactions carried out in the dark (no exposure to UV light).

Fig. 6. (A) Comparison of photocatalytic activity of various catalysts in the degradation of tetracycline under irradiation with UV light (no H_2O_2 in reaction mixture). Changes in TC concentration during the reaction and the pseudo-first-order kinetic plots are shown in Fig. S7A and B. **(B)** Reaction rate constants established for the degradation of TC via Fenton-like, photocatalytic, and photo-Fenton-like processes in the presence of CuPW-1/1 catalyst. Changes in TC concentration during the reaction and the pseudo-first-order kinetic plots are shown in Fig. S7C and D. **(C)** Reaction rate constants for different samples ($CuWO_4$, $Cu_3(PO_4)_2$, CuPW-1/1, and a physical mixture) in the photo-Fenton-like reaction. Changes in TC concentration during the reaction and the pseudo-first-order kinetic plots are shown in Fig. S7E and F. **(D)** TOC removal under different experimental conditions. *Reaction conditions*: catalyst (7.5 mg), TC solution in DI water (200 mL, 50 mg/L), H_2O_2 (50 µL, 30%), UV light, r.t., 600 rpm, without pH control (native pH ~ 4.5).

Fig. 7. Possible pathways of tetracycline degradation established based on LC-MS data and previous literature data (for more details please see Table S4).

Fig. 8. (A) The influence of scavengers on TC degradation rate in the presence of CuPW-1/1 catalyst via photo-assisted Fenton-like process. Changes in TC concentration during the reaction and the pseudo-first-order kinetic plots are shown in Fig. S9A and B. **(B)** The influence of pH on the efficiency of TC removal in the presence of CuPW-1/1 catalyst via photo-assisted Fenton-like process. Graph presenting changes in TC concentration in a function of time is shown in Fig. S9D. **(C)** The influence of water matrix (deionized water vs. tap water vs. river water from the Warta River) on the efficiency of TC degradation in the presence of CuPW-1/1 catalyst via photo-

assisted Fenton-like process. Graph presenting changes in TC concentration in a function of time is shown in Fig. S9C. **(D)** Stability and reusability of CuPW-1/1 catalyst in degradation of TC via photo-assisted Fenton-like process (reaction time: 30 min). *Reaction conditions*: catalyst (7.5 mg), TC solution in DI water (200 mL, 50 mg/L), H_2O_2 (50 µL, 30%), UV light, r.t., 600 rpm, without pH control (native pH ~ 4.5). *Recycling conditions*: catalyst (10 mg), TC solution in DI water (50 mL, 50 mg/L), H_2O_2 (25 µL), UV light, r.t., 600 rpm, without pH control (pH ~ 4.5 for A, B, and D; pH ~ 7.5 for C).

Fig. 9. Solution EPR spectra with **(A)** TEMP for the detection of singlet oxygen and **(B)** DMPO spin trap for the detection of hydroxyl radicals.

Fig. 10. Proposed photocatalytic mechanism of TC degradation in the presence of CuPW-1/1 catalyst via photo-assisted Fenton-like process established on the basis of experimental data obtained in this study.

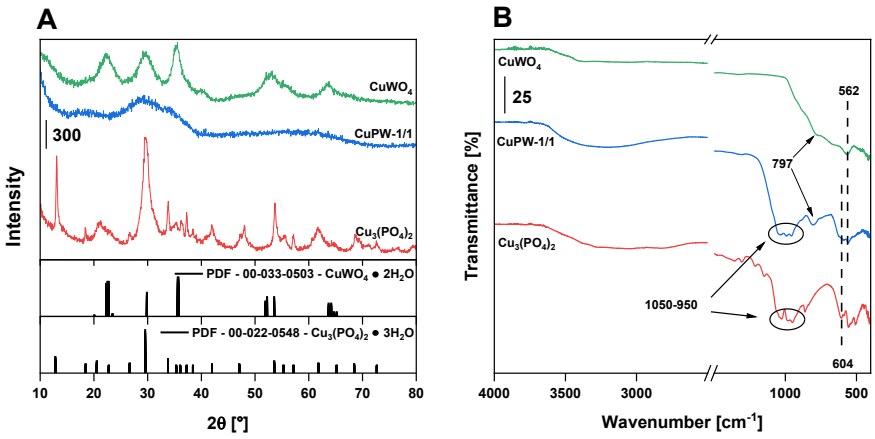

Fig. 1. (A) Powder XRD diffractograms and **(B)** ATR-FTIR spectra of the catalysts.

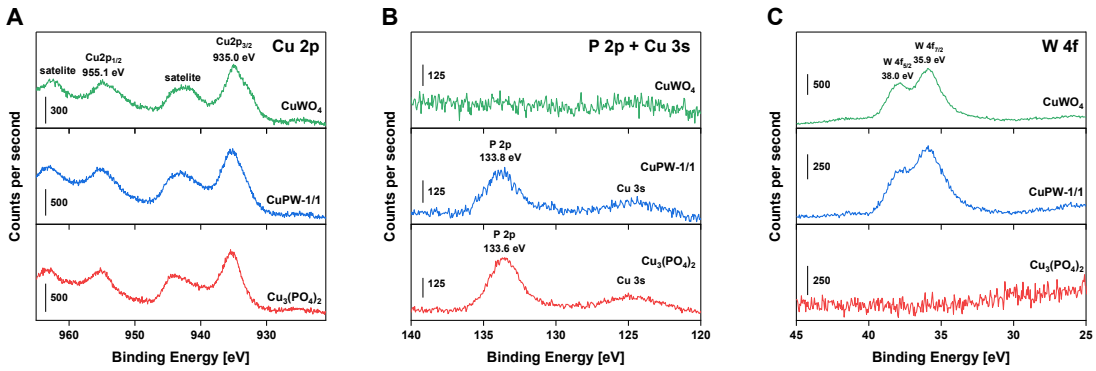

Fig. 2. XPS spectra of $CuWO_4$, $Cu_3(PO_4)_2$ and CuPW-1/1catalysts in different binding energy regions: **(A)** Cu2p, **(B)** P 2p + Cu 3s, and **(C)** W 4f.

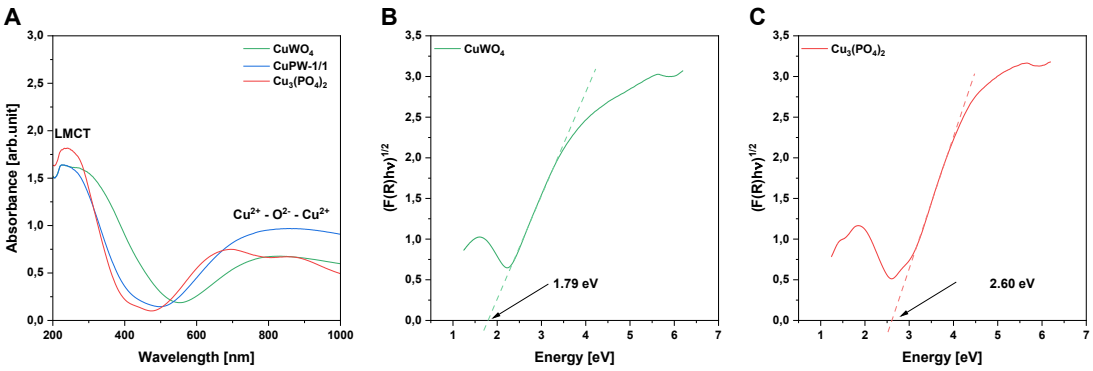

Fig. 3. (A) DR UV-vis spectra of the catalysts. Tauc's plot used for the estimation of band gap energy for **(B)** $CuWO_4$ and **(C)** $Cu_3(PO_4)_2$.

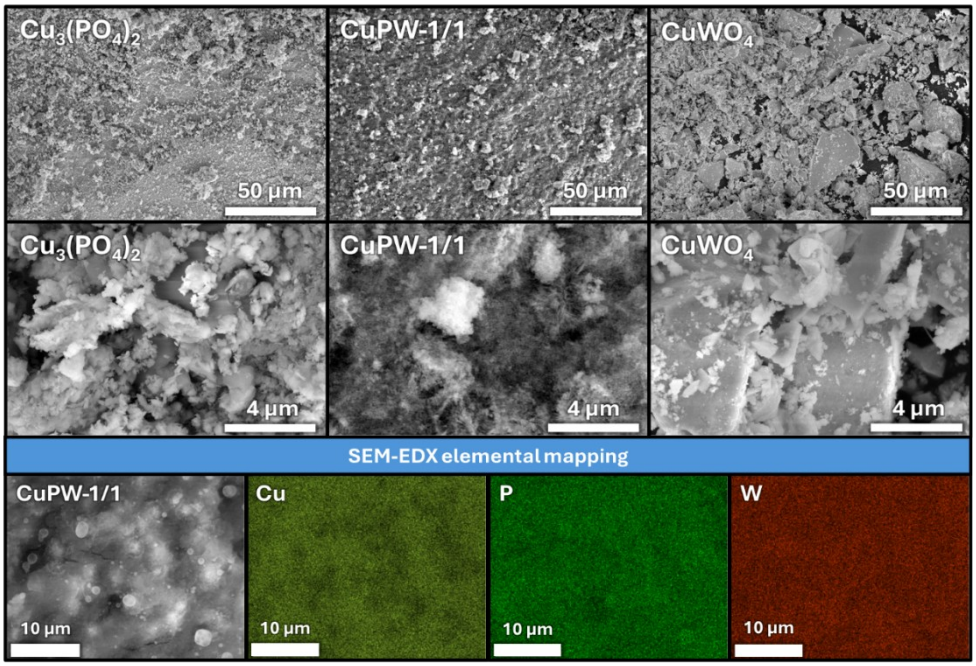

Fig. 4. Scanning Electron Microscopy analysis of synthesized catalysts combined with EDX elemental mapping of CuPW-1/1.

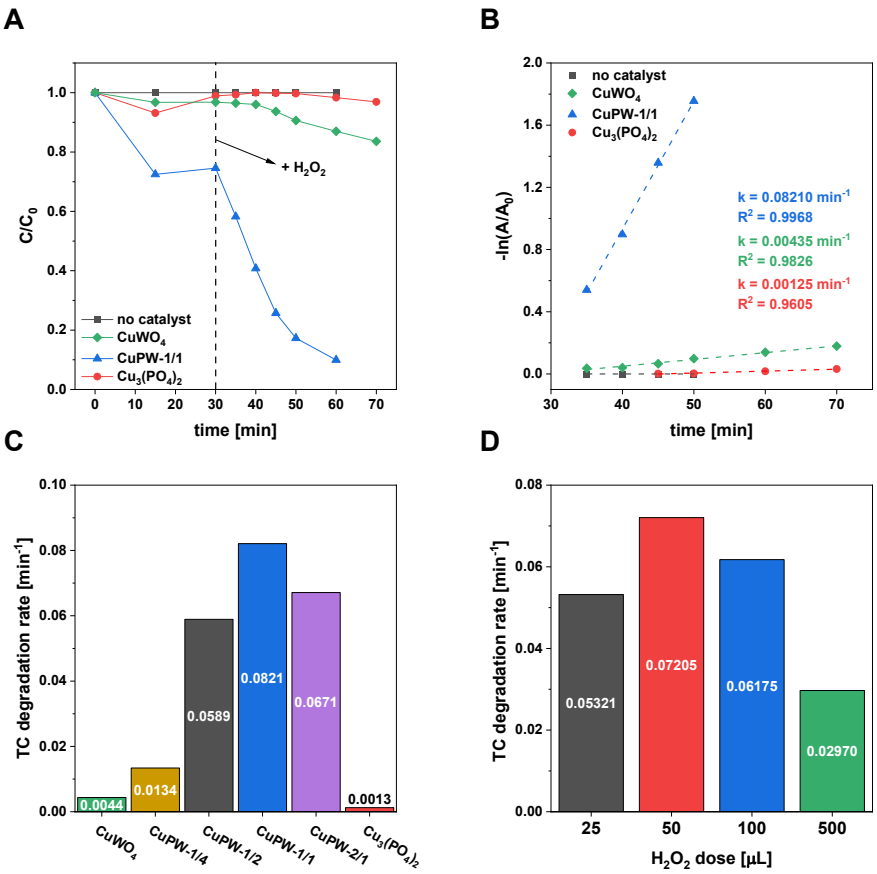

Fig. 5. (A) Efficiency of TC removal over time for $Cu_3(PO_4)_2$, $CuWO_4$ and CuPW-1/1 samples in a Fenton-like process (no exposure to UV light), including a control experiment without a catalyst. For all experiments, pre-adsorption of the pollutant was performed for 30 min before addition of H_2O_2 to assess the ability of a given catalyst to adsorb TC. Time when H_2O_2 was added to the reaction medium is marked as dashed line. **(B)** Pseudo-first order kinetics plot used to estimate TC degradation rate in the presence of investigated copper-based catalysts in a Fenton-like process. **(C)** Influence of chemical composition of CuPW composites on the TC degradation rate in the presence of H_2O_2. Pseudo-first-order kinetic plots are shown in Fig. S6A. **(D)** TC degradation rate in the presence of various concentrations of H_2O_2 for the CuPW-1/1 catalyst in a Fenton-like process. Changes in TC concentration during the reaction and the pseudo-first-order kinetic plots are shown in Fig. S6B and C, respectively. *Reaction conditions*: catalyst (15 mg), TC solution in DI water (200 mL, 50 mg/L), H_2O_2 (50 µL, or other if indicated), room temperature (r.t.), 600 rpm, without pH control (native pH ~ 4.5), all reactions carried out in the dark (no exposure to UV light).

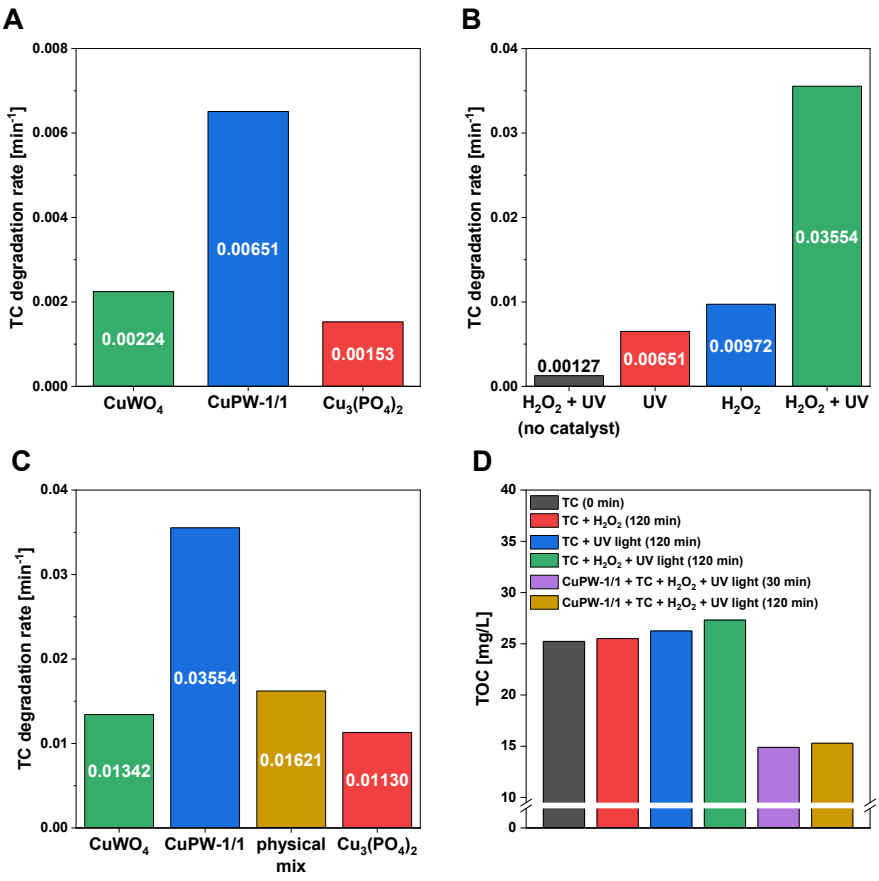

Fig. 6. (A) Comparison of photocatalytic activity of various catalysts in the degradation of tetracycline under irradiation with UV light (no H_2O_2 in reaction mixture). Changes in TC concentration during the reaction and the pseudo-first-order kinetic plots are shown in Fig. S7A and B. **(B)** Reaction rate constants established for the degradation of TC via Fenton-like, photocatalytic, and photo-Fenton-like processes in the presence of CuPW-1/1 catalyst. Changes in TC concentration during the reaction and the pseudo-first-order kinetic plots are shown in Fig. S7C and D. **(C)** Reaction rate constants for different samples ($CuWO_4$, $Cu_3(PO_4)_2$, CuPW-1/1, and a physical mixture) in the photo-Fenton-like reaction. Changes in TC concentration during the reaction and the pseudo-first-order kinetic plots are shown in Fig. S7E and F. **(D)** TOC removal under different experimental conditions. *Reaction conditions*: catalyst (7.5 mg), TC solution in DI water (200 mL, 50 mg/L), H_2O_2 (50 µL, 30%), UV light, r.t., 600 rpm, without pH control (native pH ~ 4.5).

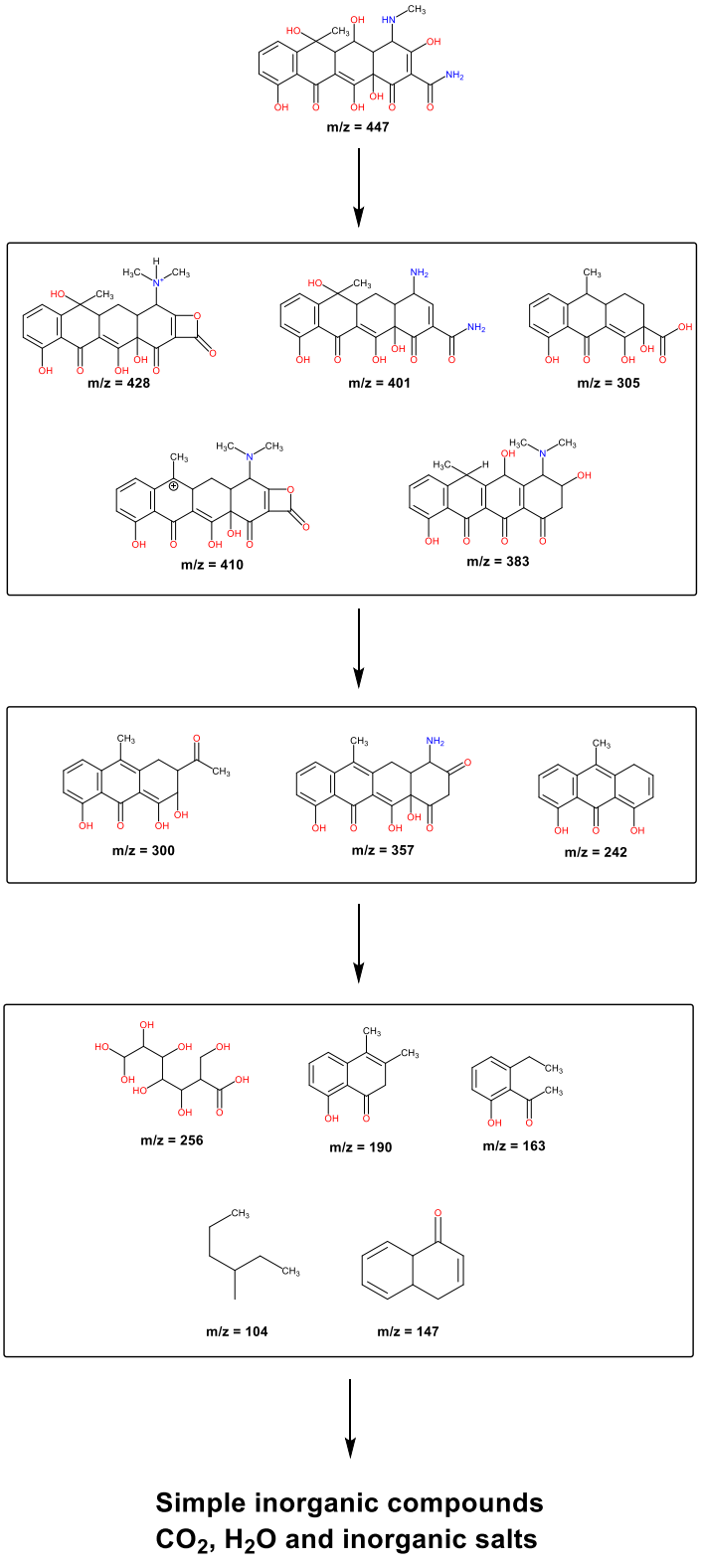

Fig. 7. Possible pathways of tetracycline degradation established based on LC-MS data and previous literature data (for more details please see Table S4).

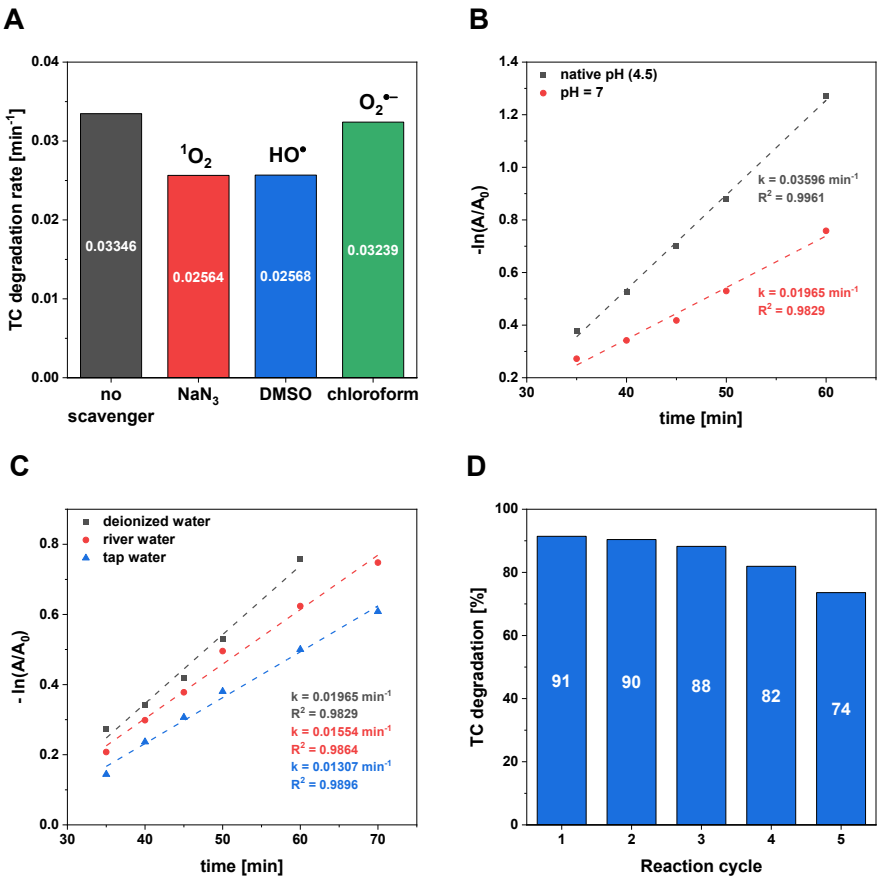

Fig. 8. (A) The influence of scavengers on TC degradation rate in the presence of CuPW-1/1 catalyst via photo-assisted Fenton-like process. Changes in TC concentration during the reaction and the pseudo-first-order kinetic plots are shown in Fig. S9A and B. **(B)** The influence of pH on the efficiency of TC removal in the presence of CuPW-1/1 catalyst via photo-assisted Fenton-like process. Graph presenting changes in TC concentration in a function of time is shown in Fig. S9D. **(C)** The influence of water matrix (deionized water vs. tap water vs. river water from the Warta River) on the efficiency of TC degradation in the presence of CuPW-1/1 catalyst via photo-assisted Fenton-like process. Graph presenting changes in TC concentration in a function of time is shown in Fig. S9C. *Reaction conditions*: catalyst (7.5 mg), TC solution in DI water (200 mL, 50 mg/L), H_2O_2 (50 µL, 30%), UV light, r.t., 600 rpm, without pH control (pH ~ 4.5 for A and B; pH ~ 7.5 for C). **(D)** Stability and reusability of CuPW-1/1 catalyst in degradation of TC via photo-assisted Fenton-like process (reaction time: 30 min). *Recycling conditions*: catalyst (10 mg), TC solution in DI water (50 mL, 50 mg/L), H_2O_2 (25 µL), UV light, r.t., 600 rpm, without pH control (native pH ~ 4.5).

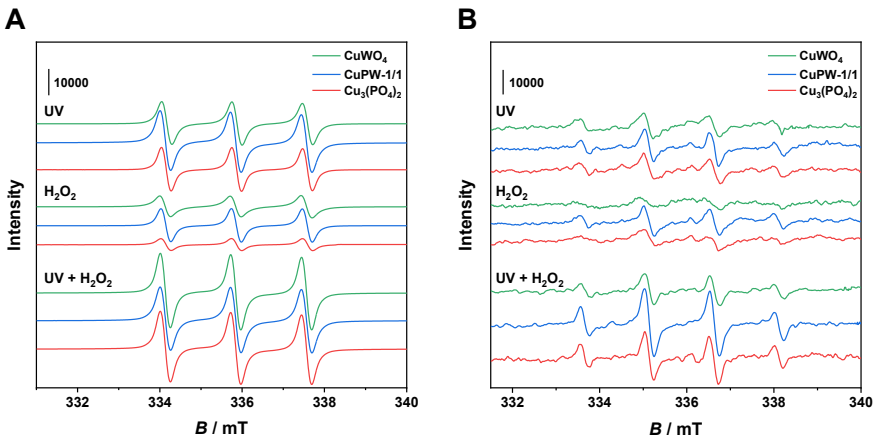

Fig. 9. Solution EPR spectra with **(A)** TEMP for the detection of singlet oxygen and **(B)** DMPO spin trap for the detection of hydroxyl radicals.

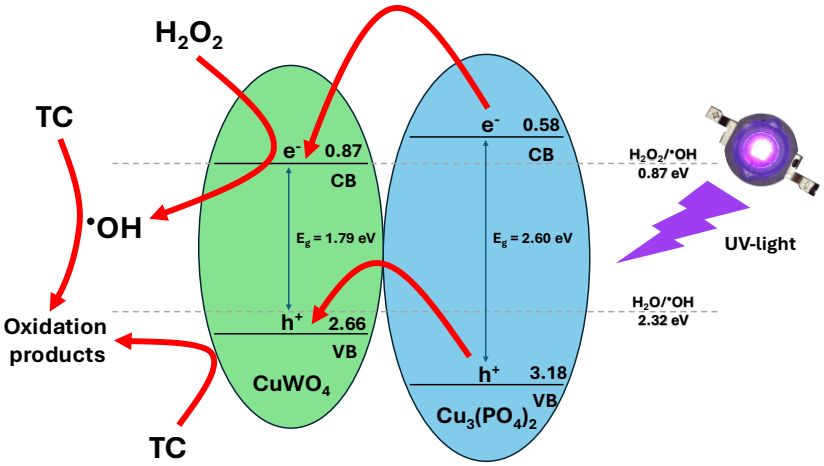

Fig. 10. Proposed photocatalytic mechanism of TC degradation in the presence of CuPW-1/1 catalyst via photo-assisted Fenton-like process established on the basis of experimental data obtained in this study.

Supplementary data

for

A facile one-pot synthesis of $Cu_3(PO_4)_2/CuWO_4$ composite for efficient degradation of tetracycline in water: Unraveling the origin of synergistic interactions between the catalyst components

Mateusz Rozmyślak[a], Kamila Sobańska[b], Grzegorz Nowaczyk[c], Adam Kubiak[a], Marcin Frankowski[a], Piotr Pietrzyk[b], Lukasz Wolski[a,*]

[a] *Faculty of Chemistry, Adam Mickiewicz University, ul. Uniwersytetu Poznańskiego 8, 61-614 Poznań, Poland*

[b] *Faculty of Chemistry, Jagiellonian University, ul. Gronostajowa 2, 30-387 Kraków, Poland*

[c] *NanoBioMedical Centre, Adam Mickiewicz University, ul. Wszechnicy Piastowskiej 3, 61-614 Poznań, Poland*

* *corresponding author: wolski.lukasz@amu.edu.pl (L. Wolski)*

Extended experimental section

Details related to the characterization of materials

The XRD patterns were recorded using a D8 Advance diffractometer (Bruker) equipped with CuKα radiation (λ = 0.154 nm), with a step size of 0.02° in the 2θ range of 10-80°.

Nitrogen adsorption-desorption isotherms were recorded using a Quantachrome instrument at -196 °C. Samples were degassed at 120 °C for 12 h before measurement. The specific surface area value was calculated using the Brunauer-Emmett-Teller (BET) method. The pore size distribution was determined from the adsorption branch of the isotherm using the BJH (Barrett-Joyner-Halenda) method.

The chemical composition of the catalysts was determined using Inductively Coupled Plasma Optical Emission Spectrometry (ICP-OES, 9820 Shimadzu, Japan). For the analysis, 50 mg of the catalyst sample was digested in 5 mL of concentrated nitric acid (HNO_3).

The morphology of the synthesized catalysts was investigated using a field-emission scanning electron microscope (FESEM) Quanta 250 FEG, FEI operating at an accelerating voltage of 10 kV. Energy-dispersive X-ray analysis (EDX) and EDX elemental mapping was performed using beam accelerating voltage of 30 kV. All measurements were conducted on a carbon adhesive conductive tape, without metallization.

For the thorough morphological characterization of materials, a high-resolution electron microscope-JEOL ARM 200F-operating at 200 kV was utilized. Samples were prepared by placing a small aliquot of dispersed powder in alcohol on grids covered with ultrathin carbon, and then allowing them to dry in low-vacuum conditions.

ATR-FTIR measurements were made using an IRSpirit-X spectrophotometer (Shimadzu, Japan) equipped with an attenuated total reflectance (QATR-S) module (Shimadzu, Japan).

The optical features of the catalysts were determined using UV-vis diffuse reflectance spectroscopy (Shimadzu UV-2600i, Japan) in a spectrophotometer equipped with an integrating sphere (ISR-2600 Integrating Sphere Attachment) covered with $BaSO_4$ as reference.

X-ray photoelectron spectroscopy (XPS) was performed using an ultra-high vacuum photoelectron spectrometer based on a Phoibos150 NAP analyzer (Specs, Germany). The analysis chamber was operated under vacuum at a pressure of approximately 5×10^{-9} mbar, and the sample was irradiated with monochromatic AlKα (1486.6 eV) radiation. Any charging that might occur during the measurements was accounted for by rigidly shifting the entire spectrum by a distance needed to set the binding energy of the C1s, assigned to adventitious carbon, to the assumed value of 284.8 eV.

To determine the surface charge of the catalysts, measurements of the zeta potential as a function of the pH of the aqueous suspensions were performed using Zetasizer Nano ZS,

Malvern, instrument. The zeta potential was estimated from electrophoretic mobility by using the Henry equation: $UE = 2\varepsilon\zeta F(ka)/3\eta$, where UE is the electrophoretic mobility, ζ the zeta potential, ε the dielectric constant, F(ka) Henry's function (set for 1.5 as in the Smoluchowski approximation), and η the viscosity. The pH value was adjusted with HCl or NaOH solutions (0.1 M). Based on the obtained results, the value of the isoelectric point (IEP) was determined by interpolating the ζ potential to zero for each of the tested samples.

EPR spectroscopy was used to identify reactive oxygen species generated after the reaction of the investigated materials with hydrogen peroxide, after irradiation, and finally after a combination of these processes. In a typical experiment, for the hydroxyl radicals identification, 0.5 mg of a catalyst was mixed with 0.5 mL of DMPO solution (4 mg/1 mL), then 0.25 mL of 1.2% H_2O_2 was added, and irradiated for 30 min (the same procedure was employed without adding H_2O_2). The mixtures prepared in this manner were transferred to a quartz capillary and the spectra were recorded with a Magnettech MS400 X-band spectrometer. The same procedure was used to identify singlet oxygen, except that 20 mM TEMP (2,2,6,6-tetramethyl-4-piperidone) was used instead of DMPO.

Details related to the catalytic tests

The TC degradation products were identified using an LC-MS/MS 8050 instrument (Shimadzu, Japan) in positive ion mode. Samples were injected into the ESI source using a SIL 30AC autosampler (1 µL injection volume) and 30/70 H_2O/ACN (1% formic acid) mobile phase. The ESI conditions were as follows: nebulizing gas flow rate: 3 L/min, heating gas flow rate: 10 L/min, drying gas flow rate: 10 L/min, interface temperature: 300 °C, DL temperature: 250 °C, heat block temperature: 400 °C. The concentration of total organic carbon (TOC) in the reaction mixtures was analyzed using a Total Organic Carbon analyzer (TOC-L) (Shimadzu, Japan).

Quenching experiments were conducted to identify the reactive oxygen species (ROS) involved in the degradation process. Sodium azide (NaN_3), chloroform, and dimethyl sulfoxide (DMSO) were used as scavengers at a concentration of 10 mmol/L. Their effects on TC removal were systematically evaluated using the same experimental conditions as presented above (catalyst dose: 7.5 mg, 200 mL of TC, concentration of the antibiotic: 50 mg/L, H_2O_2 dose: 50 µL, UV light).

Experiments using real water matrices (tap water or river water) were performed under the same conditions to assess the catalyst's effectiveness under environmentally relevant conditions. The removal efficiency of TC was determined using UV-vis spectroscopy using a selected environmentally relevant water sample as reference. The detailed composition of the real water matrices is provided in Table S2.

Additionally, the stability and reusability of the most active catalyst were examined through recycling tests. These experiments were carried out using 10 mg of the CuPW-1/1 catalyst dispersed in 50 mL of a 50 mg/L TC solution with 25 µL of H_2O_2 (stirring rate: 600 rpm, reaction time: 30 min). Each reuse test was performed at room temperature and upon exposure of the reaction media to UV light. After each cycle, the catalyst was recovered by centrifugation and reused without any further treatment.

Table S1. Mass of chemicals used for the synthesis of the catalysts via co-precipitation method and the volume of deionized water used to dissolve them. For all syntheses, volume of water used to dissolve copper(II) nitrate was adjusted to obtain 0.2 M aqueous solution of copper ions.

Catalyst	**Copper(II) nitrate trihydrate**	**Sodium phosphate dibasic**	**Sodium tungstate dihydrate**
$Cu_3(PO_4)_2$	5.71 g / 118 mL	4.5 g / 159 mL	n/a
CuPW-2/1	2.69 g / 55 mL	1.51 g / 53 mL	1.06 g / 16 mL
CuPW-1/1	2.30 g / 47 mL	0.90 g / 32 mL	1.56 g / 24 mL
CuPW-1/2	1.96 g / 40 mL	0.45 g / 16 mL	1.90 g / 29 mL
CuPW-1/4	1.74 g / 36 mL	0.23 g / 8mL	1.96 g / 30 mL
$CuWO_4$	2.33 g / 48 mL	n/a	3.18 g / 48 mL

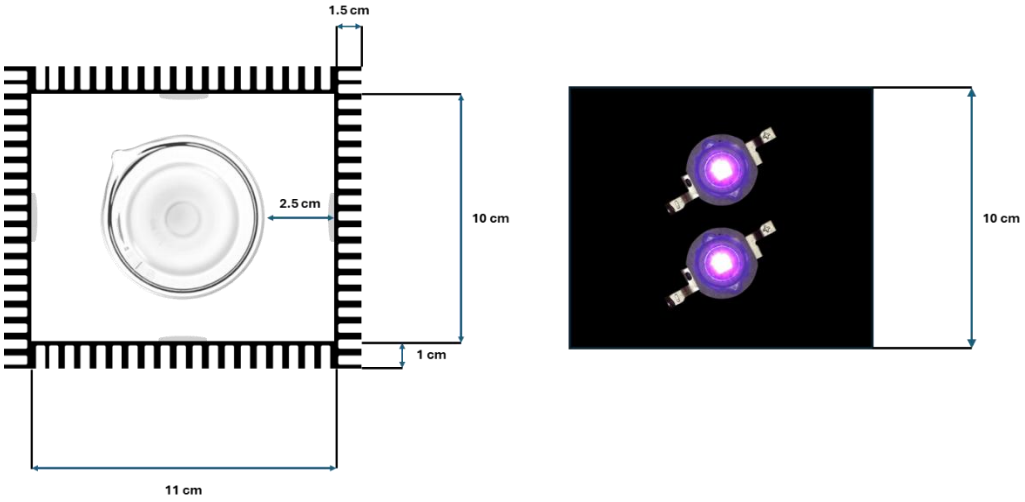

Fig. S1. Schematic representation and top view of the experimental photoreactor setup. Each wall was equipped with two 3W LEDs (λ = 365 and 380 nm).

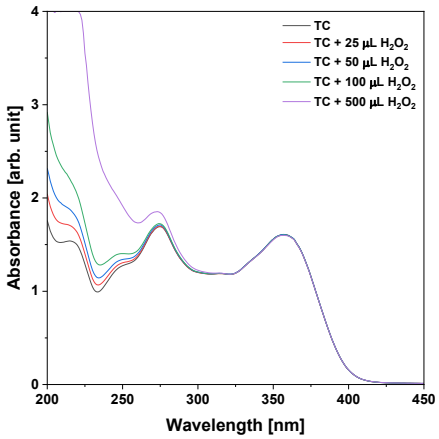

Fig. S2. UV-vis spectra of TC solution (200 mL, 50 mg/L) with varied hydrogen peroxide dose.

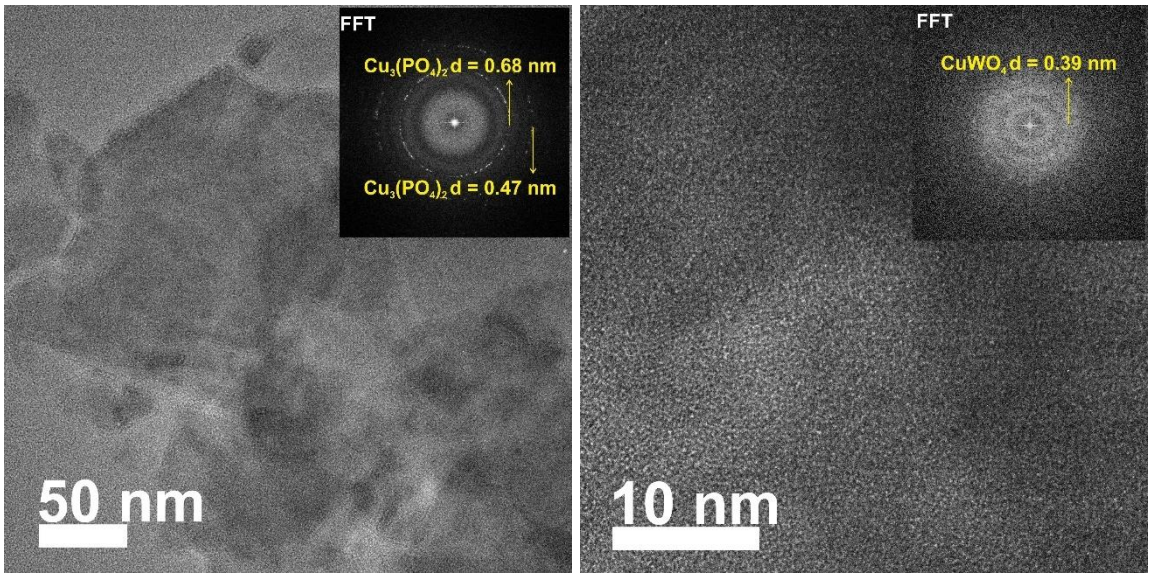

Fig. S3. TEM images and FFT analysis of $CuWO_4$ and $Cu_3(PO_4)_2$ catalysts.

Table S2. Chemical composition of the catalysts determined based on ICP-OES measurements. Loading of copper(II) phosphate was determined based on phosphorus content in the catalysts.

Catalyst	**$Cu_3(PO_4)_2$ [wt.%]**	**$CuWO_4$ [wt.%]**
CPW-1/4	13.12	86.88
CPW-1/2	31.08	68.92
CPW-1/1	51.57	48.43
CPW-2/1	63.29	36.71

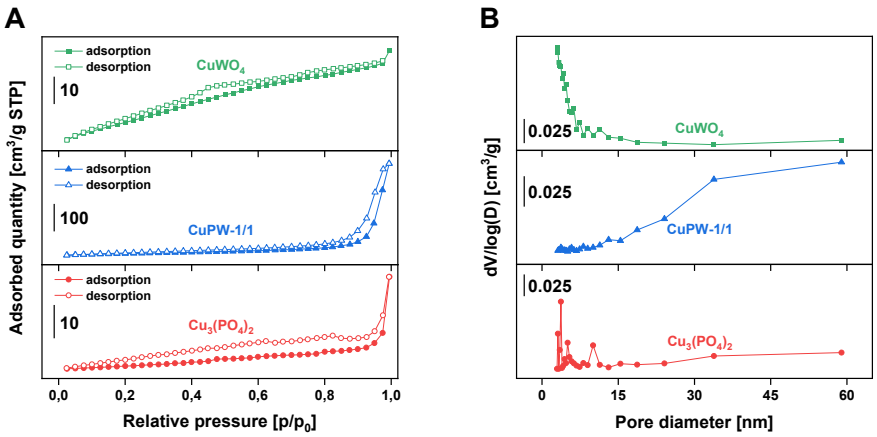

Fig. S4. (A) Nitrogen adsorption-desorption isotherms and **(B)** pore size distribution for the catalysts.

Table S3. BET surface area and average pore size determined for the catalysts from adsorption branch of the isotherm using BJH method.

Catalyst	**BET Surface area [m^2/g]**	**Average pore diameter [nm]**
$Cu_3(PO_4)_2$	7.6	3.7
CuPW-2/1	54.4	3.1
CuPW-1/1	58.6	33.3
CuPW-1/2	54.2	33.3
$CuWO_4$	81.9	3.1

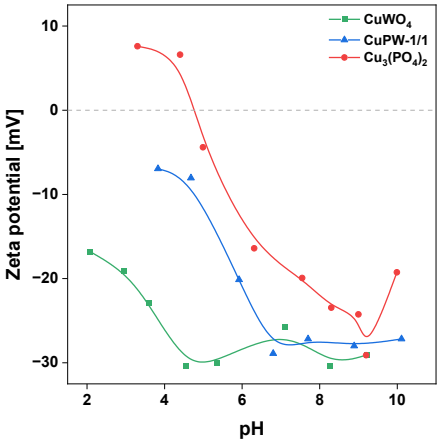

Fig. S5. Zeta potential measurements for the catalysts at different pH values.

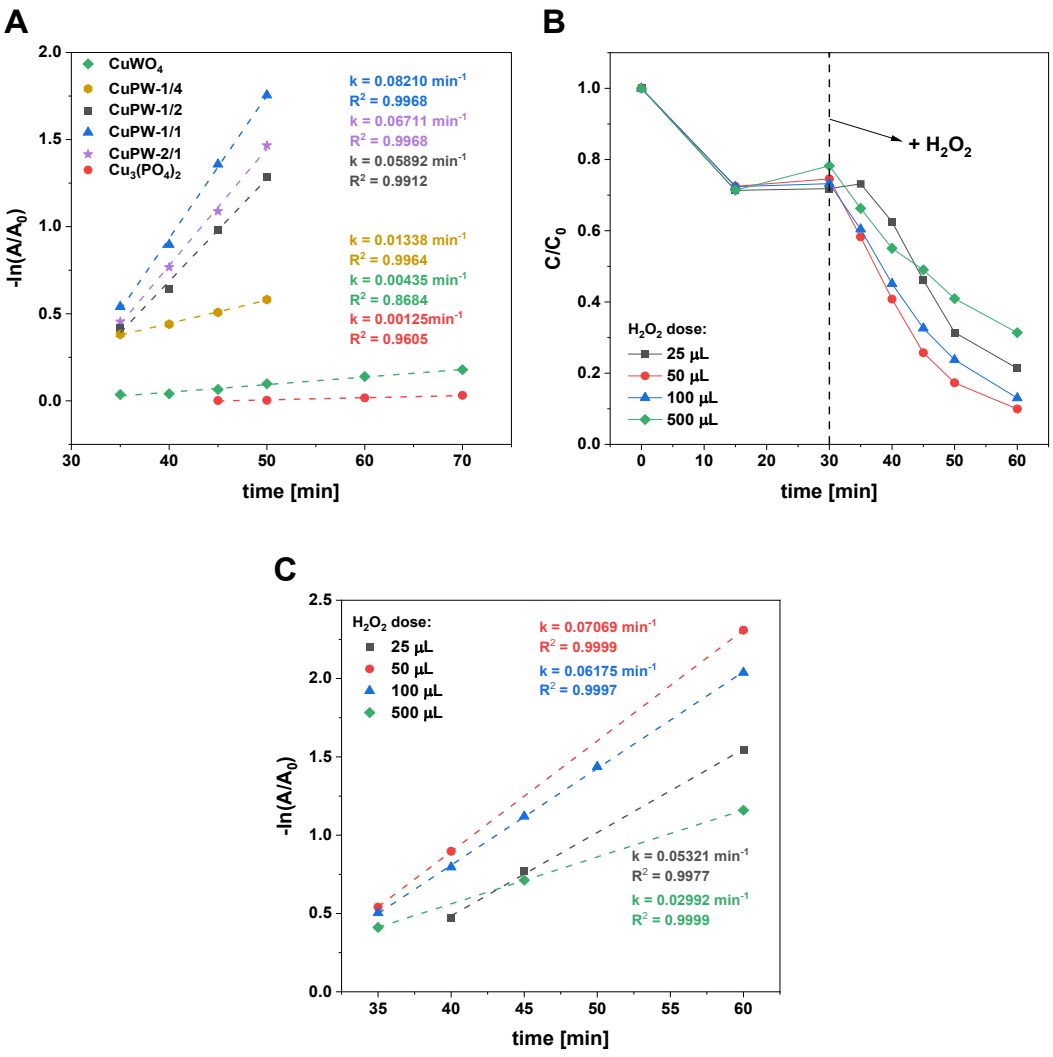

Fig. S6. (A) Pseudo-first-order kinetic plot demonstrating the effect of catalyst composition on the degradation rate of tetracycline in a Fenton-like process. **(B)** Graph presenting changes in TC concentration in a function of time for the experiment aimed as assessing the influence of H_2O_2 dose on the efficiency of TC degradation in a Fenton-like process using CuPW-1/1 composite as a catalyst. **(C)** Pseudo-first-order plot for the determination of the apparent degradation rate of TC at different H_2O_2 doses in a Fenton-like process. *Reaction conditions*: catalyst (15 mg), TC solution in DI water (200 mL, 50 mg/L), H_2O_2 (50 µL, or other if indicated), r.t., 600 rpm, experiment without pH control (native pH ~ 4.5), all experiments carried out in the dark (no exposure to UV light).

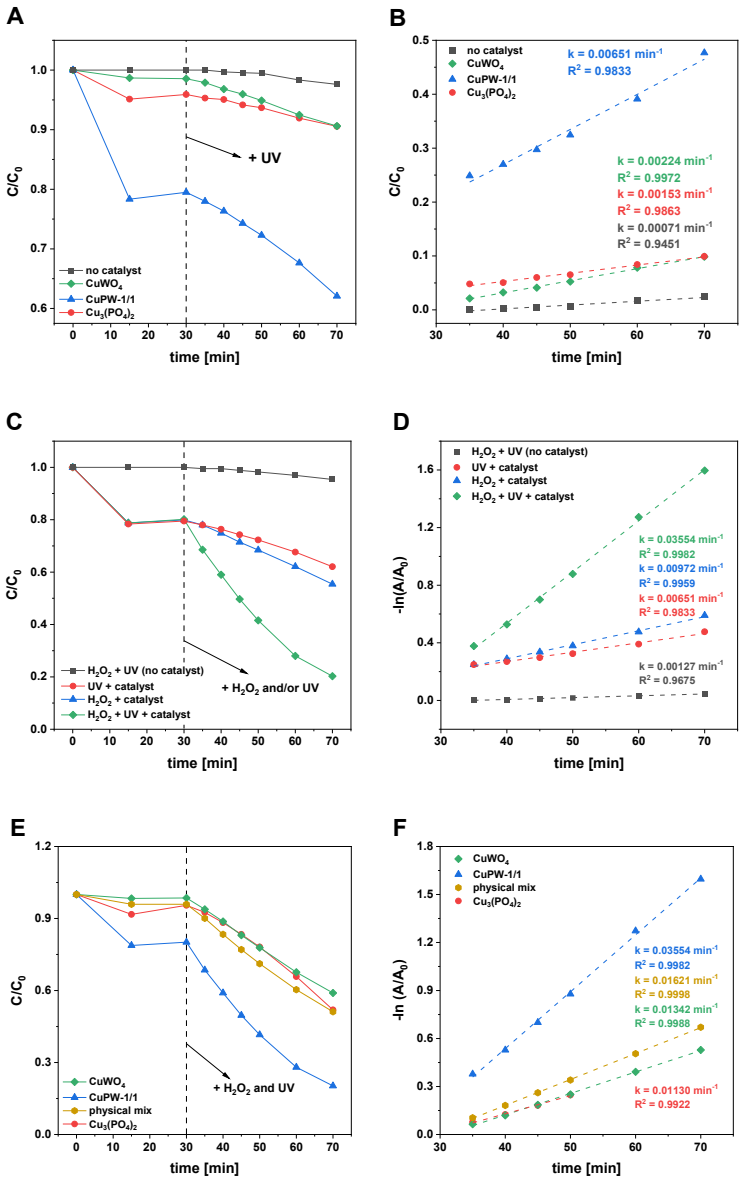

Fig. S7. (A) Graph presenting changes in TC concentration in a function of time for the experiment aimed at assessing the photocatalytic activity of different catalysts. **(B)** Pseudo-first-order plot for the determination of the apparent degradation rate of TC in a photocatalytic process. **(C)** Graph presenting changes in TC concentration in a function of time for the experiment aimed at assessing the influence of oxidation conditions (UV vs. H_2O_2 vs. H_2O_2 + UV) on the efficiency of TC degradation in the presence of CuPW-1/1 catalyst. **(D)** Pseudo-first-order plot for the determination of the apparent degradation rate of TC via different oxidation conditions using CuPW-1/1 catalyst. **(E)** Graph presenting changes in TC concentration in a function of time for the experiment aimed as assessing the influence of the catalyst on the efficiency of TC degradation via photo-Fenton-like process. **(F)** Pseudo-first-order plot for the determination of the apparent degradation rate of TC in the presence of various catalysts via photo-Fenton-like process. *Reaction conditions*: catalyst (7.5 mg), TC solution in DI water (200 mL, 50 mg/L), H_2O_2 (50 µL, 30%), UV-light, r.t., 600 rpm, experiment without pH control (native pH ~ 4.5).

TC

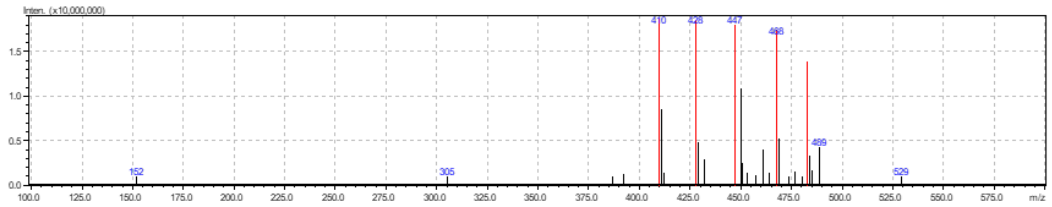

TC + H_2O_2 + light – 2 hours

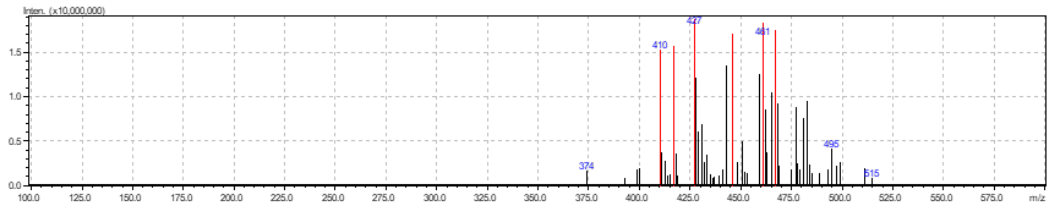

TC + catalyst + H_2O_2 + light – 30 minutes

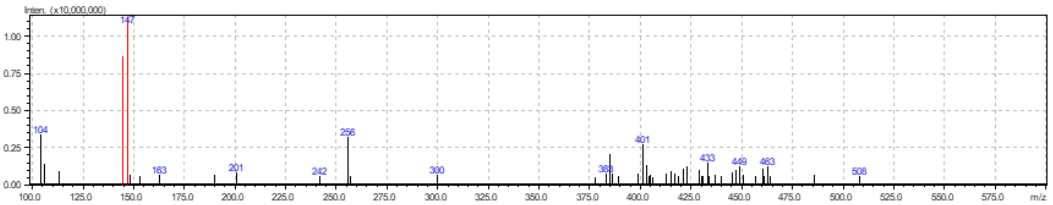

TC + catalyst + H_2O_2 + light – 60 minutes

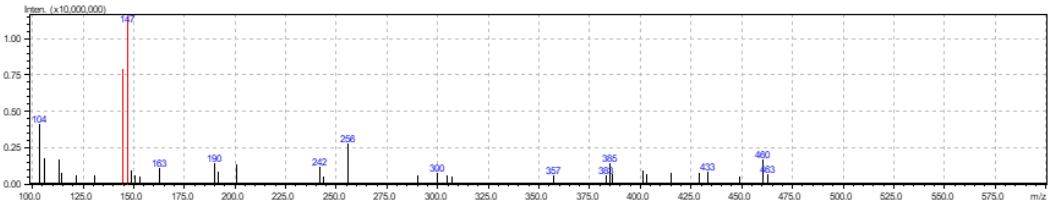

Fig. S8. LC-MS results. Reaction conditions: catalyst (7.5 mg), TC solution in DI water (200 mL, 50 mg/L), H_2O_2 (50 µL, 30%), UV light, r.t., 600 rpm, without pH control (native pH ~ 4.5).

Table S4. Proposed structures of TC degradation products formed in the presence of CuPW-1/1 in a photo-assisted Fenton-like process. The structures were identified based on results obtained from LC-MS studies in a positive mode and previous literature data.

m/z	Chemical formula	Reference
104	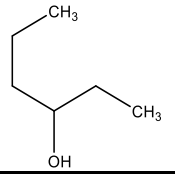	[1]
147	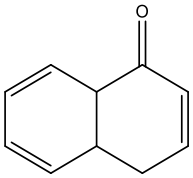	[2]
163	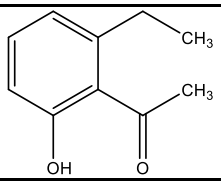	[3]
190	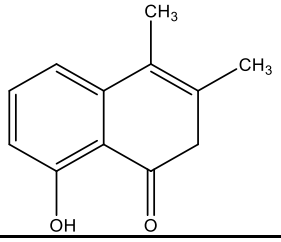	[3]
242	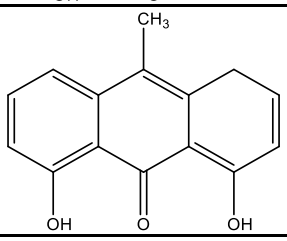	[3]
256	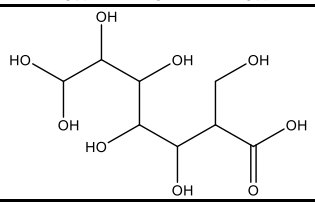	[4]
300	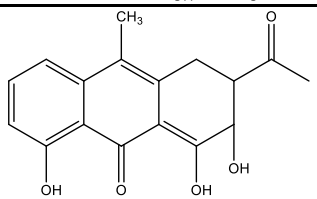	[5]
305	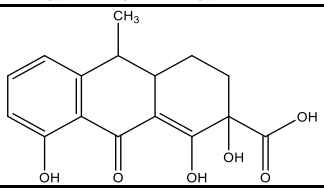	[6]

357	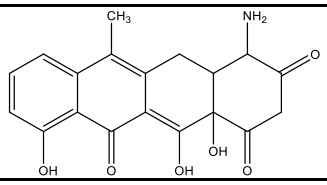	[3]
383	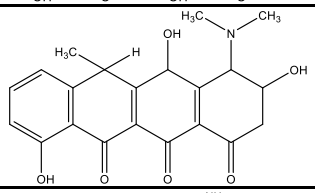	[7]
401	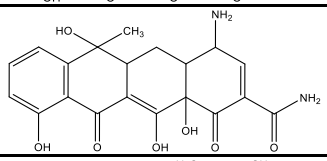	[8]
410	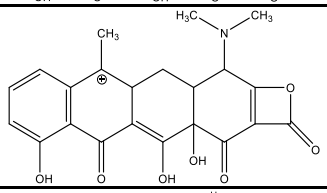	[9]
428	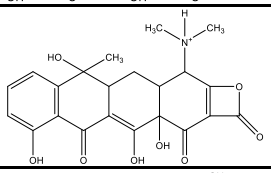	[9]
447	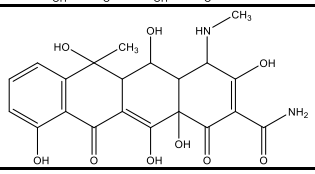	[10]

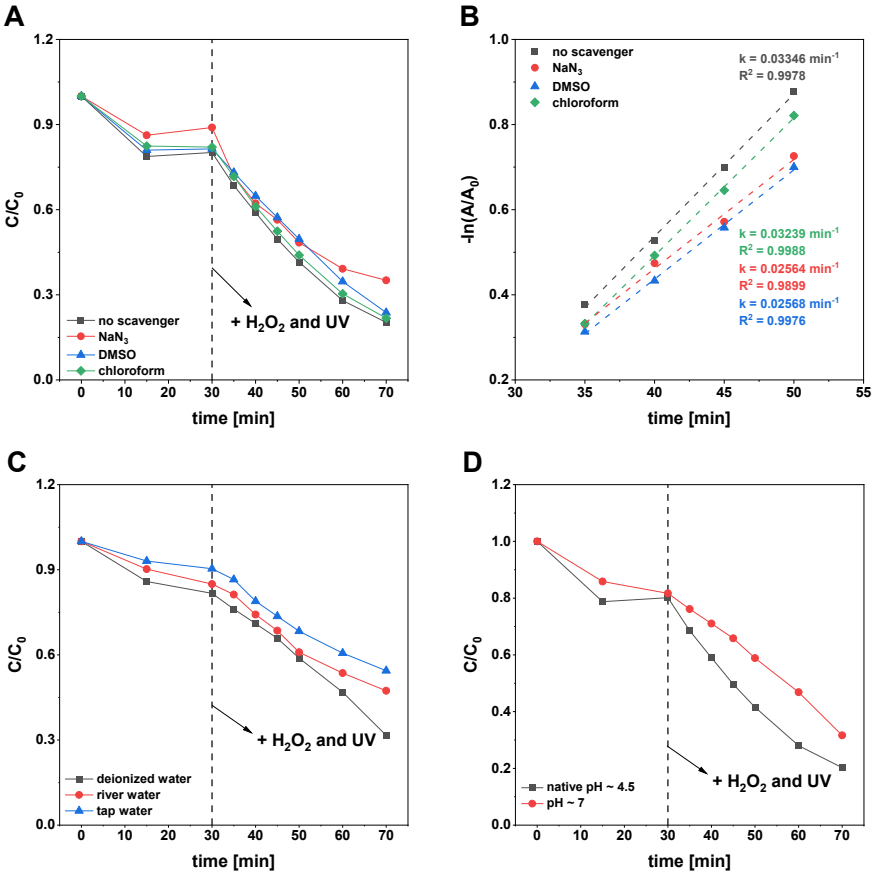

Fig. S9. (A,B) Graph presenting changes in TC concentration in a function of time for the experiment aimed at assessing the effect of radical scavengers on the degradation of TC via photo-assisted Fenton-like process. **(C)** The influence of water matrix (deionized water vs. tap water vs. river water from the Warta River) on the efficiency of TC degradation in the presence of CuPW-1/1 catalyst via photo-assisted Fenton-like process. **(D)** Graph presenting changes in TC concentration in a function of time for the experiment aimed at assessing the influence of pH on the efficiency of TC removal in the presence of CuPW-1/1 catalyst via photo-assisted Fenton-like process. *Reaction conditions*: catalyst (7.5 mg), TC solution in DI water (200 mL, 50 mg/L), H_2O_2 (50 µL, 30%), UV light, r.t., 600 rpm, without pH control (pH ~ 4.5 for A, B and D, pH ~ 7.5 for C).

Table S5. Electron affinity and first ionization energy of elements from the literature data [11].

Element	**Electron affinity (EA) [eV]**	**First ionization energy (IE) [eV]**
Cu	1.23	7.72
P	0.74	10.48
W	0.82	7.98
O	1.46	13.61

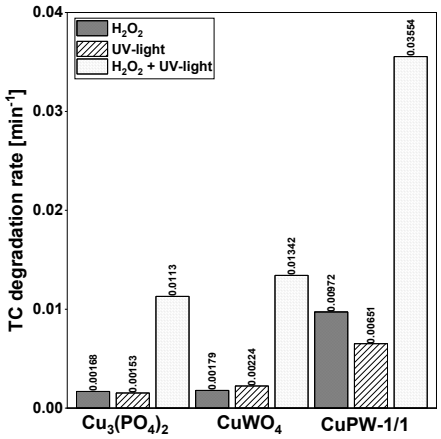

Fig. S10. Comparison of TC degradation rates in the presence of $Cu_3(PO_4)_2$, $CuWO_4$, and CuPW-1/1 via Fenton-like, photocatalytic and photo-assisted Fenton-like processes. *Reaction conditions*: catalyst (7.5 mg), TC solution in DI water (200 mL, 50 mg/L), H_2O_2 (50 μL, 30%), UV-light, r.t., 600 rpm, experiment without pH control (native pH ~ 4.5).

Table S6. Chemical composition of tap and river water. Concentration of metals was determined based on ICP-OES measurements (Shimadzu, Japan). Total organic carbon, total carbon, and inorganic carbon were determined using TOC analyzer (Shimadzu, Japan). Total nitrogen was determined using TOC analyzer equipped with a total nitrogen unit (Shimadzu, Japan).

Parameter	Tap water	River water
pH	7.45	7.80
Ca [mg/L]	120.1	79.8
Mg [mg/L]	13.21	9.37
Na [mg/L]	33.9	45.1
K [mg/L]	5.95	91.71
Total organic carbon [mg/L]	-	0.64
Total carbon [mg/L]	53.79	47.78
Inorganic carbon [mg/L]	53.79	47.14
Total nitrogen [mg/L]	0.74	3.48

Tap water collected in Morasko (Poznań, Poland).

River water collected from the Warta River (Owińska, Poland).

Table S7. Concentration of Cu, W, and P in post reaction mixtures established based on ICP-OES measurements.

Reaction cycle	**Cu**	**P**	**W**
	[mg/L]		
Recycling[a] – 1st cycle	13.1	4.54	13.71
Recycling – 2nd cycle	14.2	4.02	7.75
Recycling – 3rd cycle	11.1	3.05	4.83
Recycling – 4th cycle	8.12	2.26	3.29
Recycling – 5th cycle	4.46	1.24	1.75
After reaction with the use of river water[b]	1.59	0.93	4.47

[a] Reaction conditions: catalyst (10 mg), TC solution in DI water (50 mL, 50 mg/L), H_2O_2 (25 µL), UV light, r.t., 600 rpm, without pH control (pH ~ 4.5)

[b] Reaction conditions: catalyst (7.5 mg), TC solution in DI water (200 mL, 50 mg/L), H_2O_2 (50 µL, 30%), UV light, r.t., 600 rpm, without pH control (pH ~ 7.5)

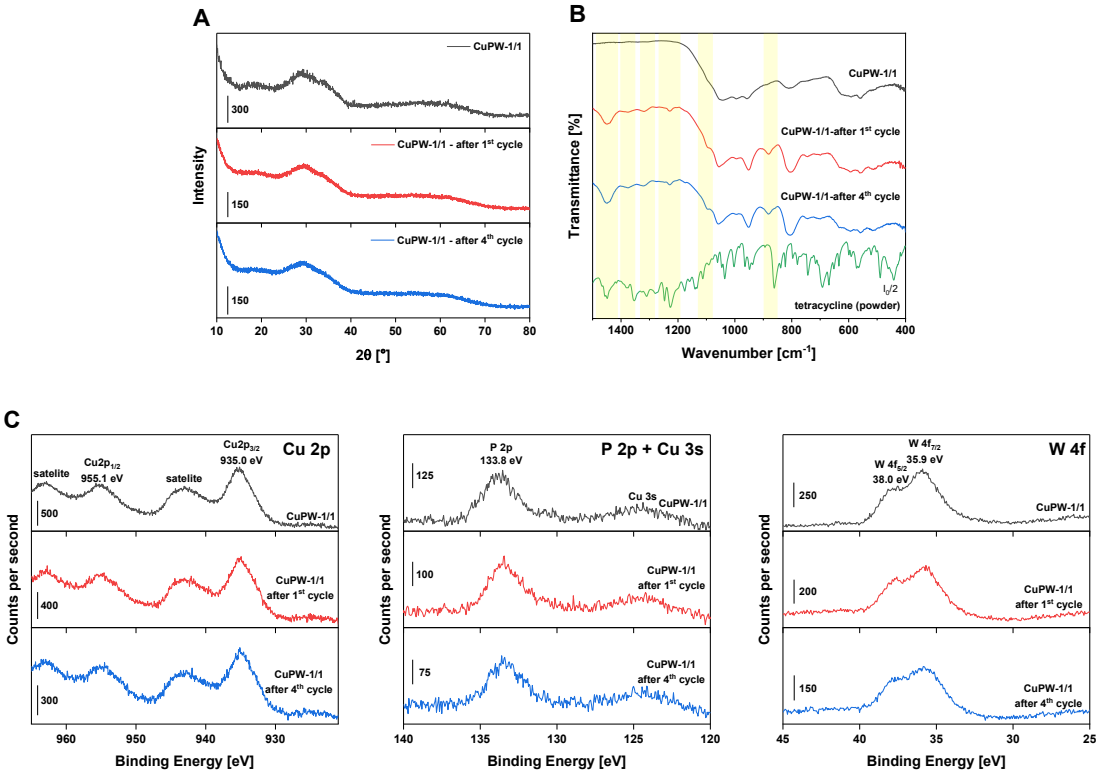

Fig. S11. (A) XRD, **(B)** ATR-FTIR, and **(C)** XPS data for fresh and reused CuPW-1/1 composite catalyst after 1st and 4th reaction cycle. Before XRD, ATR-FTIR and XPS measurements the spent catalyst was separated from the reaction mixture, washed with deionized water and dried for 20 h at 80°C without any additional treatment. In the case of ATR-FTIR spectra, some new IR bands were observed for the spent catalyst and assigned to the presence of adsorbed TC molecules and/or its degradation products (IR bands highlighted in yellow).

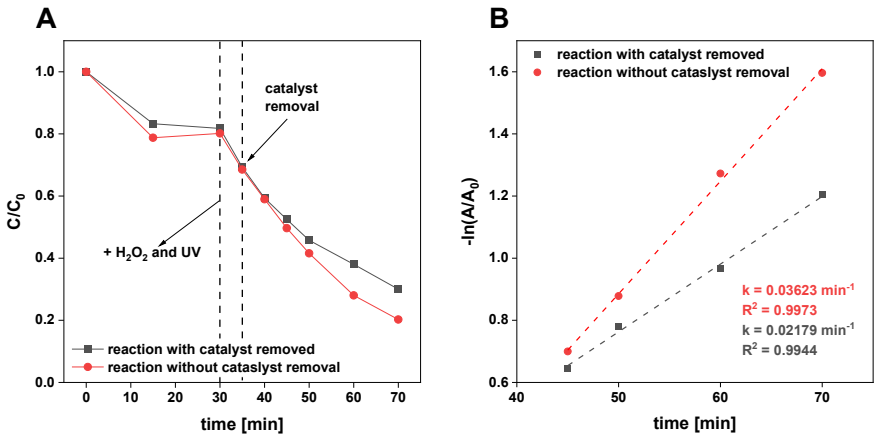

Fig. S12. (A) The influence of catalyst removal on the efficiency of tetracycline degradation via photo-assisted Fenton-like process. The catalyst was separated from the reaction mixture by filtration, and the resulting filtrate was transferred into a clean beaker to continue the reaction. **(B)** Pseudo-first-order plot for the determination of the apparent degradation rate of TC after separation of the catalyst by filtration. Reaction without separation of the catalyst is provided for comparison purposes. *Reaction conditions*: catalyst (7.5 mg), TC solution in DI water (200 mL, 50 mg/L), H_2O_2 (50 µL, 30%), UV-light, r.t., 600 rpm, experiment without pH control (native pH ~ 4.5).

References

[1] L. Song, Q. Fang, Q. Yang, X. Fu, Y. Lu, T. Cai, M. Zou, Q. Zeng, Efficient activation of peracetic acid by multi-valent Cu_7S_4 for the degradation and detoxication of tetracycline hydrochloride: Cu^{3+} acts as an active site, J. Water Process Eng. 57 (2024) 104715, https://doi.org/10.1016/j.jwpe.2023.104715.

[2] K.-P. Cui, Y.-Y. He, K.-J. Xu, Y. Zhang, C.-B. Chen, Z.-J. Xu, X. Chen, Degradation of Tetracycline Hydrochloride by Cu-Doped MIL-101(Fe) Loaded Diatomite Heterogeneous Fenton Catalyst, Nanomaterials 12 (2022) 811, https://doi.org/10.3390/nano12050811.

[3] Y. Xia, X. Li, Y. Wu, Z. Chen, Z. Pi, A. Duan, J. Liu, Tetracycline hydrochloride degradation by activation of peroxymonosulfate with lanthanum copper Ruddlesden-Popper perovskite oxide: Performance and mechanism, Chemosphere 332 (2023) 138906, https://doi.org/10.1016/j.chemosphere.2023.138906.

[4] S. Wu, H. Hu, Y. Lin, J. Zhang, Y.H. Hu, Visible light photocatalytic degradation of tetracycline over TiO_2, Chem. Eng. J. 382 (2020) 122842, https://doi.org/10.1016/j.cej.2019.122842.

[5] X. Zhang, C. Shi, H. Hu, Z. Zhou, X. Zhao, Complexation and degradation of tetracycline by activation of molecular oxygen with biochar-supported nano-zero-valent copper composite, Environ. Sci. Pollut. Res. 30 (2023) 34827–34839, https://doi.org/10.1007/s11356-022-24489-1.

[6] J. Guo, L. Jiang, J. Liang, W. Xu, H. Yu, J. Zhang, S. Ye, W. Xing, X. Yuan, Photocatalytic degradation of tetracycline antibiotics using delafossite silver ferrite-based Z-scheme photocatalyst: Pathways and mechanism insight, Chemosphere 270 (2021) 128651, https://doi.org/10.1016/j.chemosphere.2020.128651.

[7] A.M. Kamel, H.G. Fouda, P.R. Brown, B. Munson, Mass spectral characterization of tetracyclines by electrospray ionization, H/D exchange, and multiple stage mass spectrometry, J. Am. Soc. Mass Spectrom. 13 (2002) 543–557, https://doi.org/10.1016/S1044-0305(02)00356-2.

[8] A.A. Borghi, M.S.A. Palma, Tetracycline: Production, waste treatment and environmental impact assessment, Brazilian J. Pharm. Sci. 50 (2014) 25–40, https://doi.org/10.1590/S1984-82502011000100003.

[9] I. Dalmázio, M.O. Almeida, R. Augusti, T.M.A. Alves, Monitoring the degradation of tetracycline by ozone in aqueous medium via atmospheric pressure ionization mass spectrometry, J. Am. Soc. Mass Spectrom. 18 (2007) 679–687, https://doi.org/10.1016/j.jasms.2006.12.001.

[10] W.R. Chen, C.H. Huang, Transformation kinetics and pathways of tetracycline antibiotics with manganese oxide, Environ. Pollut. 159 (2011) 1092–1100, https://doi.org/10.1016/j.envpol.2011.02.027.

[11] J.P. Fuentes, S. Jadoun, O. Yepsen, H.D. Mansilla, J. Yáñez, Prediction of band edge potentials and reaction products in photocatalytic copper and iron sulfides, Photochem. Photobiol. Sci. 22 (2023) 1855–1864, https://doi.org/10.1007/s43630-023-00415-3.